PREPARATION AND OPERATIONS OF THE MISSION PERFORMANCE CENTRE (MPC) FOR THE COPERNICUS SENTINEL-3 MISSION

S3-A OLCI Cyclic Performance Report

Cycle No. 015

Start date: 26/02/2017

End date: 25/03/2017

SENTINEL 3

Mission Performance Centre

Ref.: S3MPC.ACR.PR.01-015
Issue: 1.0
Date: 31/03/2017
Contract: 4000111836/14/I-LG

Customer:	ESA	**Document Ref.:**	S3MPC.ACR.PR.01-015
Contract No.:	4000111836/14/I-LG	**Date:**	31/03/2017
		Issue:	1.0

Project:	PREPARATION AND OPERATIONS OF THE MISSION PERFORMANCE CENTRE (MPC) FOR THE COPERNICUS SENTINEL-3 MISSION		
Title:	S3-A OLCI Cyclic Performance Report		
Author(s):	OLCI ESLs		
Approved by:	L. Bourg, OLCI ESL Coordinator	**Authorized by**	Frédéric Rouffi, OPT Technical Performance Manager
Distribution:	ESA, EUMETSAT, S3MPC consortium		
Accepted by ESA	S. Dransfeld, MPC Deputy TO for OPT P. Féménias, MPC TO		
Filename	S3MPC.ACR.PR.01-015 - i1r0 - OLCI Cyclic Report 015.docx		

Changes Log

Version	Date	Changes
1.0	31/03/2017	First Version

List of Changes

Version	Section	Answers to RID	Changes

Table of content

List of Figures

1 Instrument monitoring

1.1 CCD temperatures

The monitoring of the CCD temperatures is based on MPMF data extractions not yet operational. In the meantime, we monitor the CCD temperatures on the long-term using Radiometric Calibration Annotations (see Figure 1). Variations are very small (0.08 C peak-to-peak) and no trend can be identified. Data from current cycle (rightmost data points) do not show any specificity.

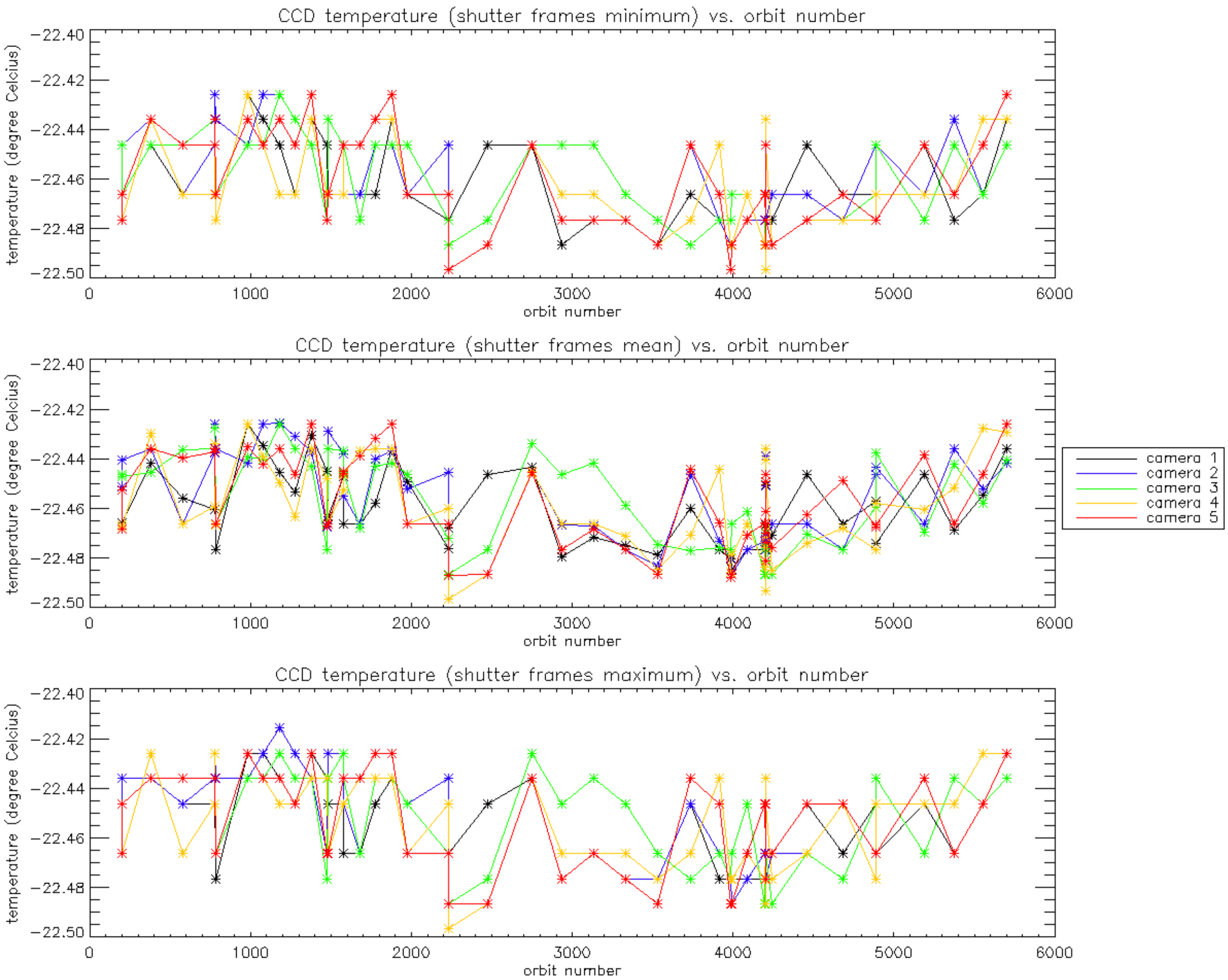

Figure 1: long term monitoring of CCD temperatures using minimum value (top), time averaged values (middle), and maximum value (bottom) provided in the annotations of the Radiometric Calibration Level 1 products, for the Shutter frames, all radiometric calibrations so far.

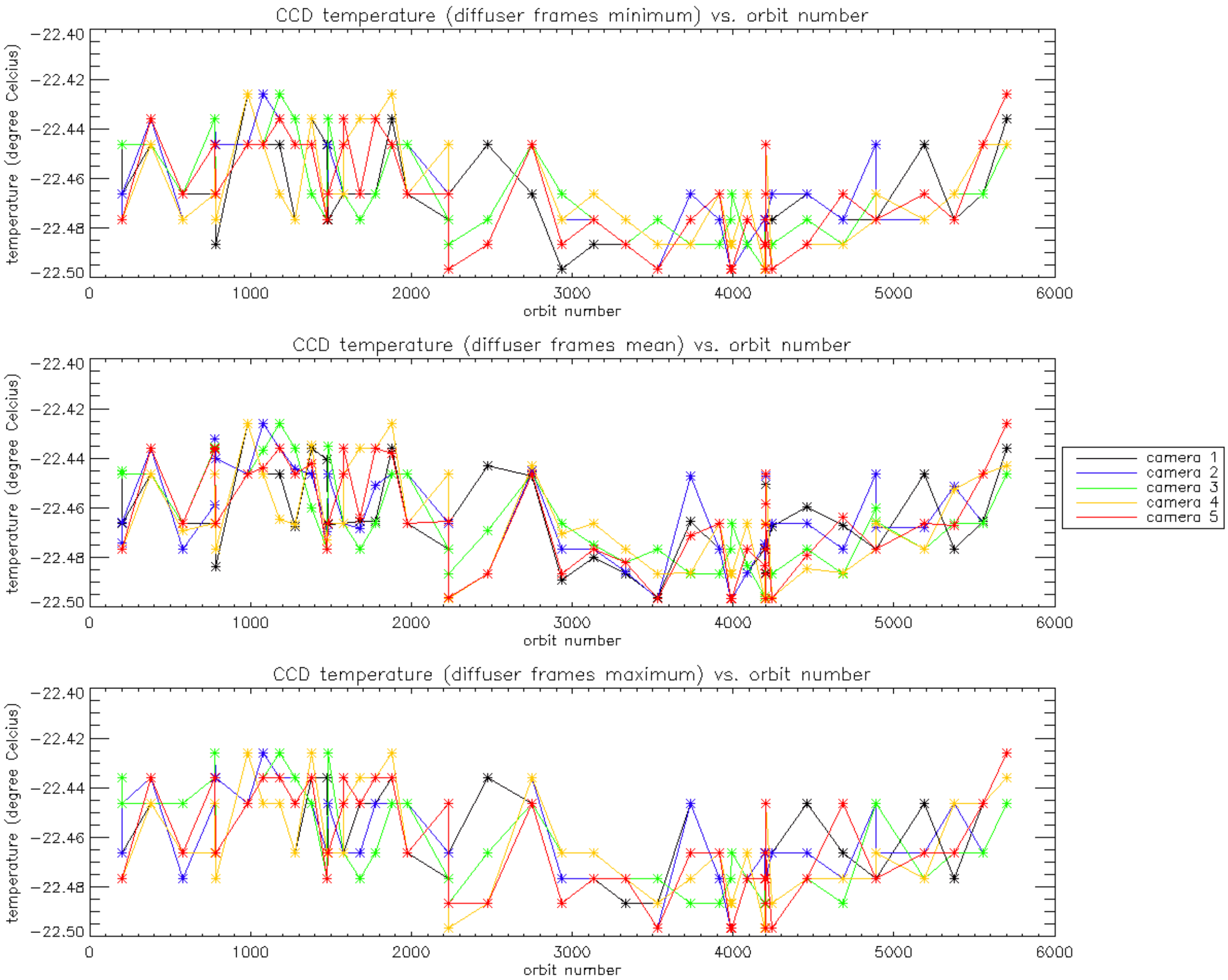

Figure 2: Same as Figure 1 for diffuser frames.

1.2 Radiometric Calibration

Three OLCI Radiometric Calibration Sequences have been acquired during Cycle 015:

- S01 sequence on 27/02/2017 12:39 to 12:41 (absolute orbit 5372)
- S01 sequence on 12/03/2017 08:38 to 08:40 (absolute orbit 5555)
- S01 sequence on 22/03/2017 14:21 to 14:23 (absolute orbit 5701)

The acquired Sun azimuth angles are presented on below, on top of the nominal values without Yaw Manoeuvre (i.e. with nominal Yaw Steering control of the satellite).

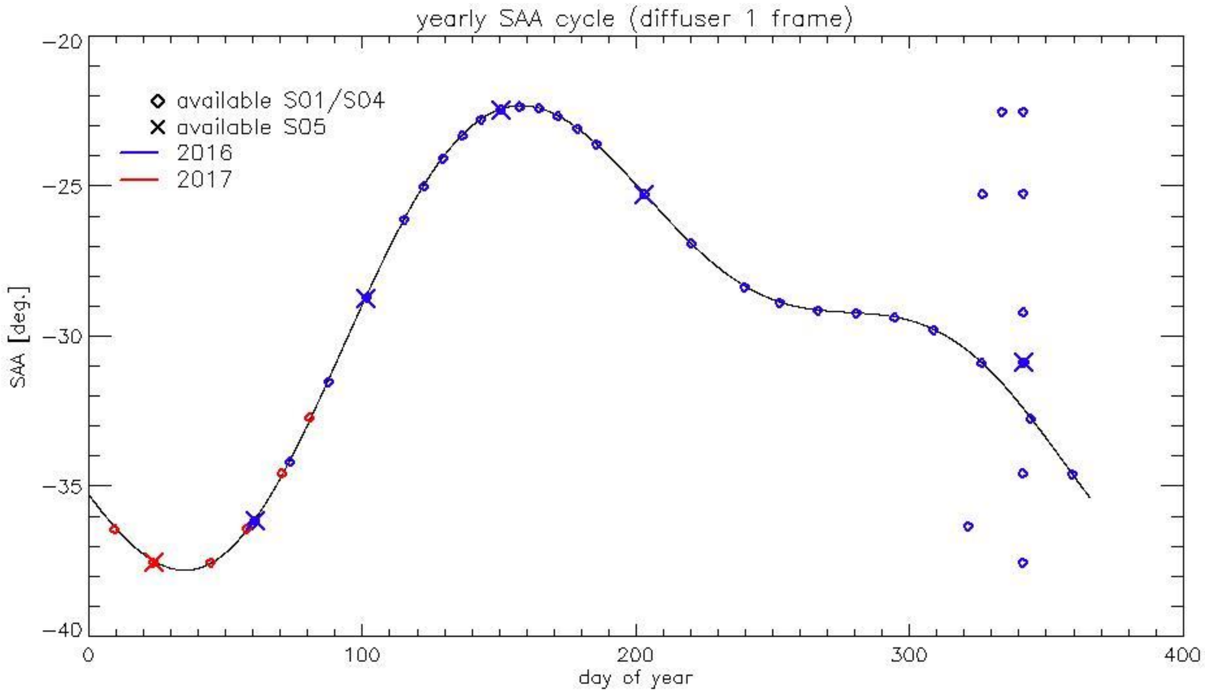

Figure 3: Sun azimuth angles during acquired Radiometric Calibrations (diffuser frame) on top of nominal yearly cycle (black curve). Diffuser 1 with diamonds, diffuser 2 with crosses, 2016 acquisitions in blue, 2017 (current cycle) in red.

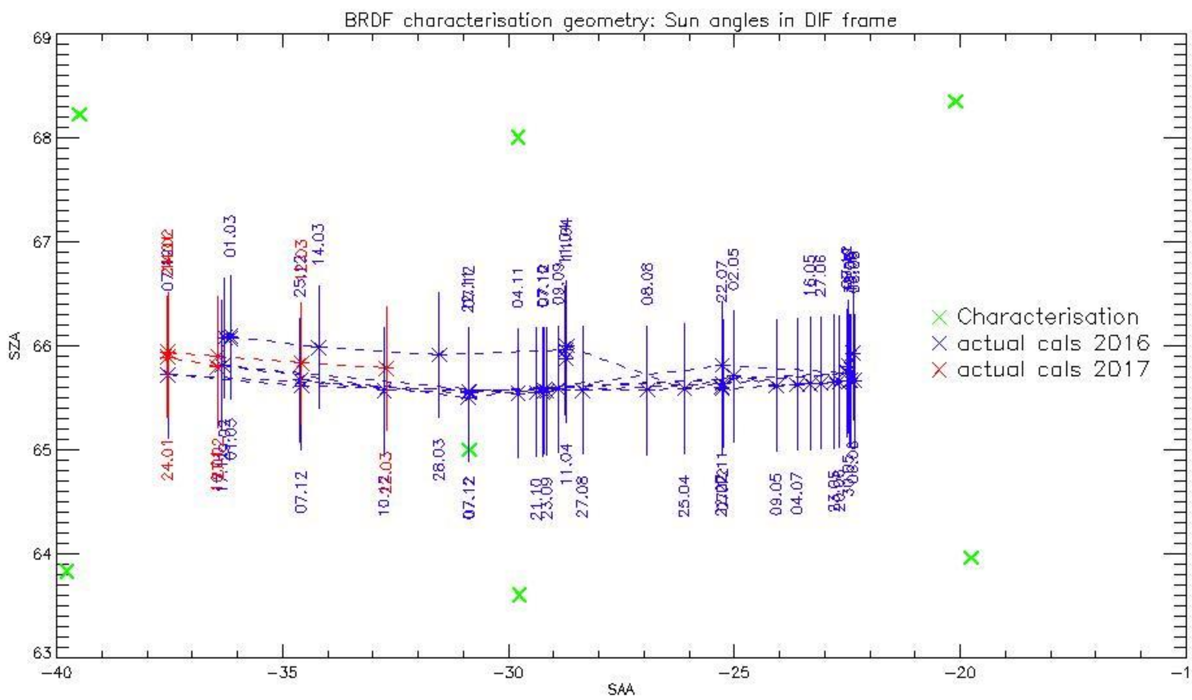

Figure 4: Sun geometry during radiometric Calibrations on top of characterization ones (diffuser frame)

This section presents the overall monitoring of the parameters derived from radiometric calibration data and highlights, if present, specificity of current cycle data.

1.2.1 Dark Offsets [OLCI-L1B-CV-230]

Dark offsets

Dark offsets are continuously affected by the global offset induced by the Periodic Noise on the OCL convergence. Current Cycle calibrations (orbits 4685, 4887 & 4888) are affected the same way as others. The amplitude of the shift varies with band and camera from virtually nothing (e.g. camera 2, band 0a1) to up to 5 counts (Oa21, camera 3). The Periodic Noise itself comes on top of the global shift with its known signature: high frequency oscillations with a rapid damp. This effect remains more or less stable with time in terms of amplitude, frequency and decay length, but its phase varies with time, introducing the global offset mentioned above.

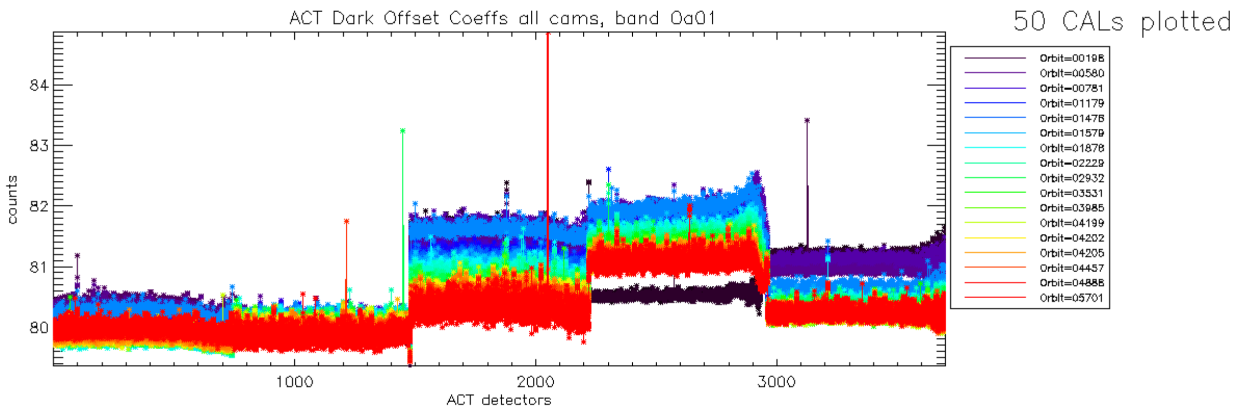

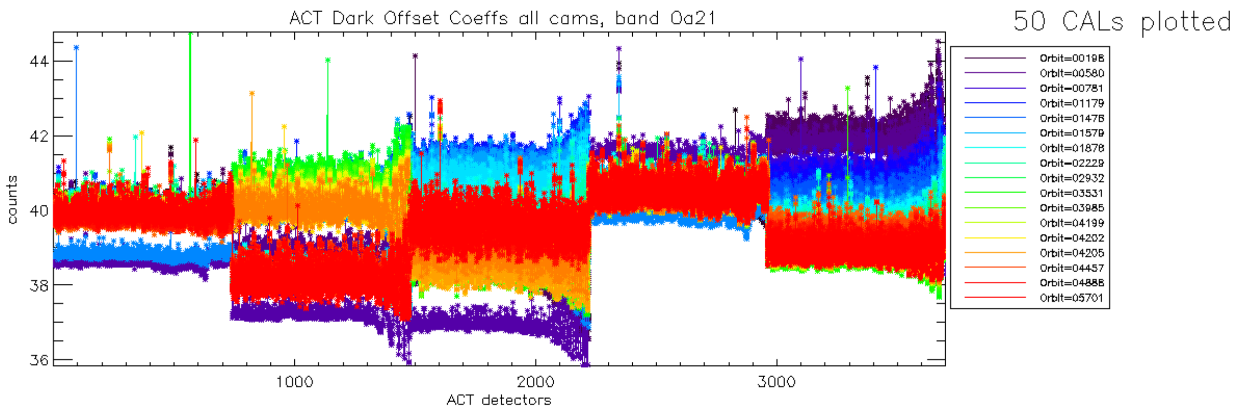

Figure 5: Dark Offset for band Oa1 (top) and Oa21 (bottom), all radiometric calibrations so far except the first one (orbit 183) for which the instrument was not thermally stable yet.

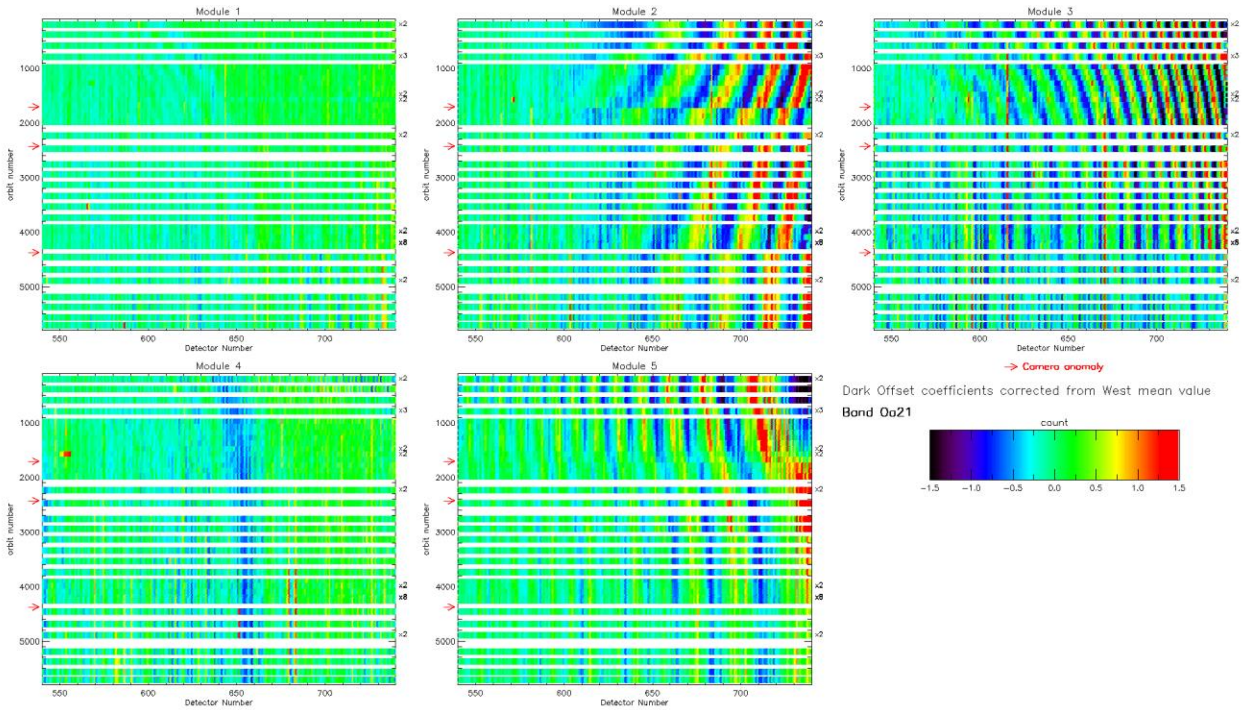

Figure 6: map of periodic noise for the 5 cameras, for band Oa21. X-axis is detector number (East part, from 540 to 740, where the periodic noise occurs), Y-axis is the orbit number. The counts have been corrected from the west detectors mean value (not affected by periodic noise). Periodic noise amplitude is high in camera 2, 3 and 4. It is lower in camera 4 and small in camera 1.

Looking at Figure 5 shows no significant evolution of this parameter during the current cycle. Figure 6 shows that since the last sudden PN change (phase and amplitude) caused by the camera 2 anomaly at orbit 4364 (18 December 2016), PN is nearly stabilized again. (See in particular cameras 2, 3 & 5).

Dark Currents

Dark Currents are not affected by the global offset of the Dark Offsets, thanks to the clamping to the average blind pixels value. However, the oscillations of Periodic Noise remain visible. There is no significant evolution of this parameter during the current cycle.

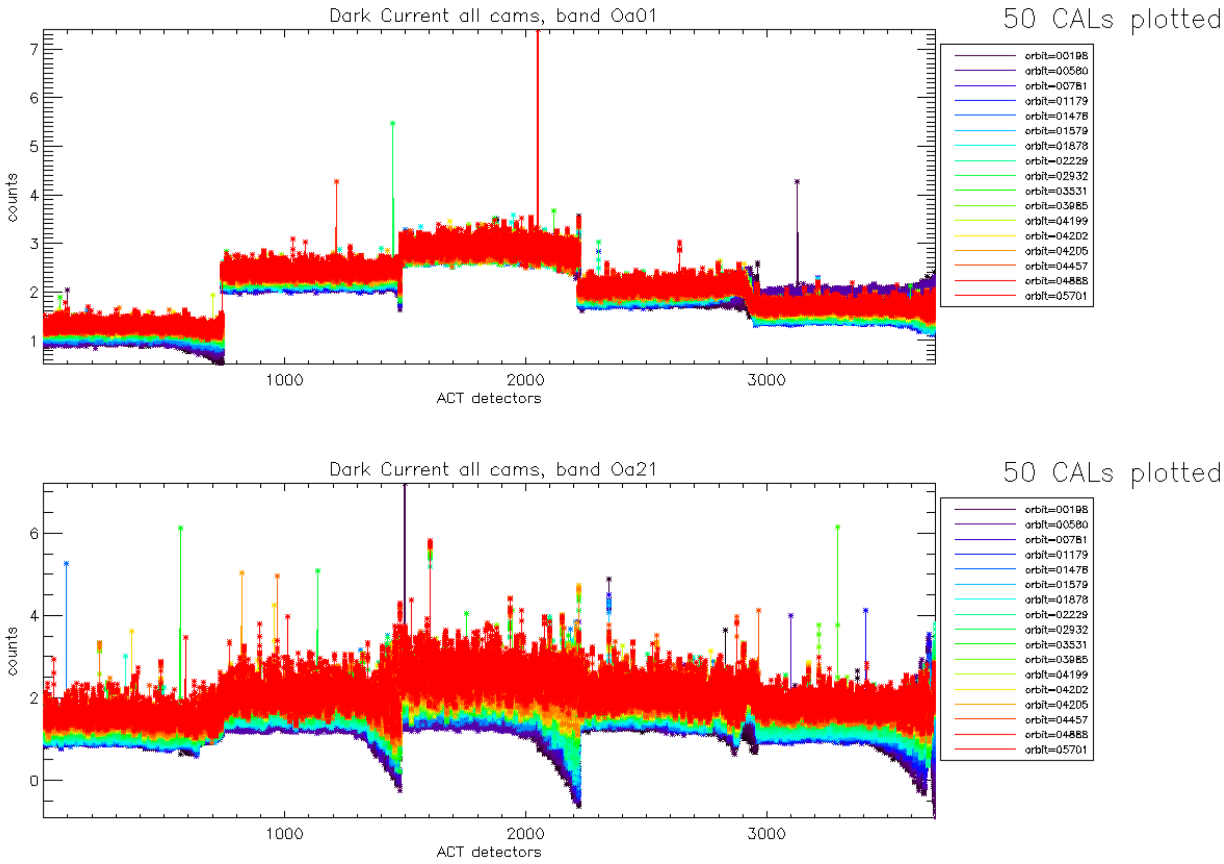

Figure 7: Dark Current for band Oa1 (top) and Oa21 (bottom), all radiometric calibrations so far except the first one (orbit 183) for which the instrument was not thermally stable yet.

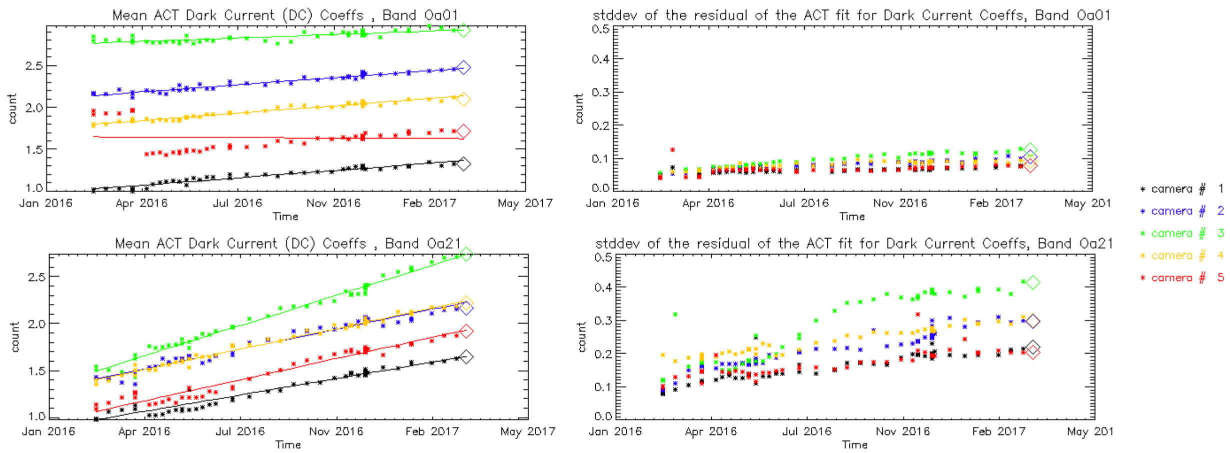

Figure 8: left column: ACT mean on 400 first detectors of Dark Current coefficients for spectral band Oa01 (top) and Oa21 (bottom). Right column: same as left column but for Standard deviation instead of mean. We see an increase of the DC level as a function of time especially for band Oa21. A possible explanation could be the increase of the number of hot pixels which is more important in Oa21 because this band is made of more CCD lines than band Oa01 and thus receives more cosmic rays impacts. It is known that cosmic rays degrade the structure of the CCD, generating more and more hot pixels at long term scales.

1.2.2 Instrument response and degradation modelling [OLCI-L1B-CV-250]

Figure 9 below shows the gain coefficients of every pixel for two OLCI channels, Oa1 (400 nm) and Oa21 (1020 nm), highlighting the significant evolution of the instrument response since early mission.

Figure 10 on the other hand displays the time evolution of the cross-track averaged gain, for each module, as a function of time. It shows that if a significant evolution occurred during the early mission, the trends tend to stabilize, with a noticeable exception during the Yaw Manoeuvres (YM) and after, pointing at the dependency of the BRDF model performance with Sun azimuth (on purpose large variations during YM, due to the shape of the seasonal cycle since then). In particular all calibrations between beginning of August and early December (YM) provide very stable results, within 0.5% for all bands. This is further illustrated on Figure 11. The latter shows that radiometric gains are becoming very stable over this period but starts to vary again when the first Yaw Manoeuvre tests come into play, illustrating the influence of geometry. Calibrations acquired during the current cycle, acquired with nominal Yaw Steering, confirm these findings.

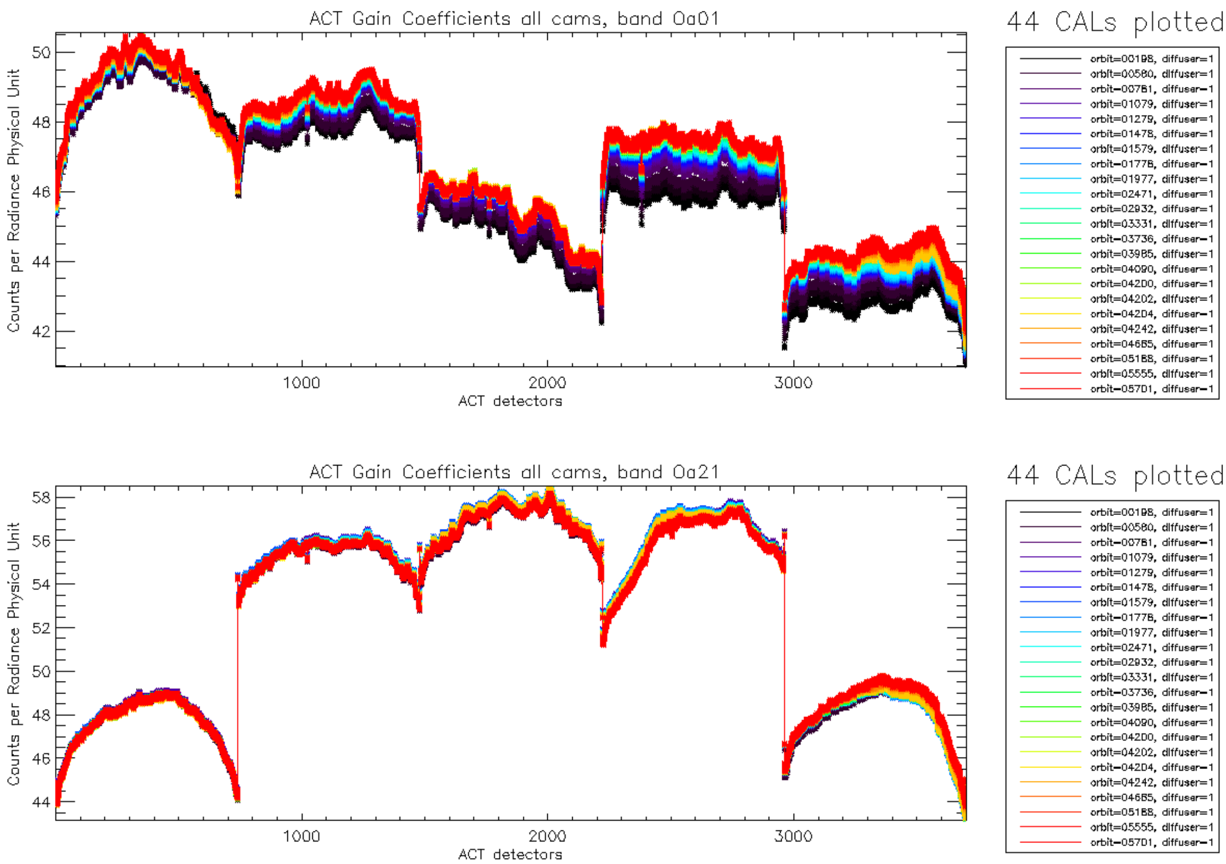

Figure 9: Gain Coefficients for band Oa1 (top) and Oa21 (bottom), all diffuser 1 radiometric calibrations so far except the first one (orbit 183) for which the instrument was not thermally stable yet.

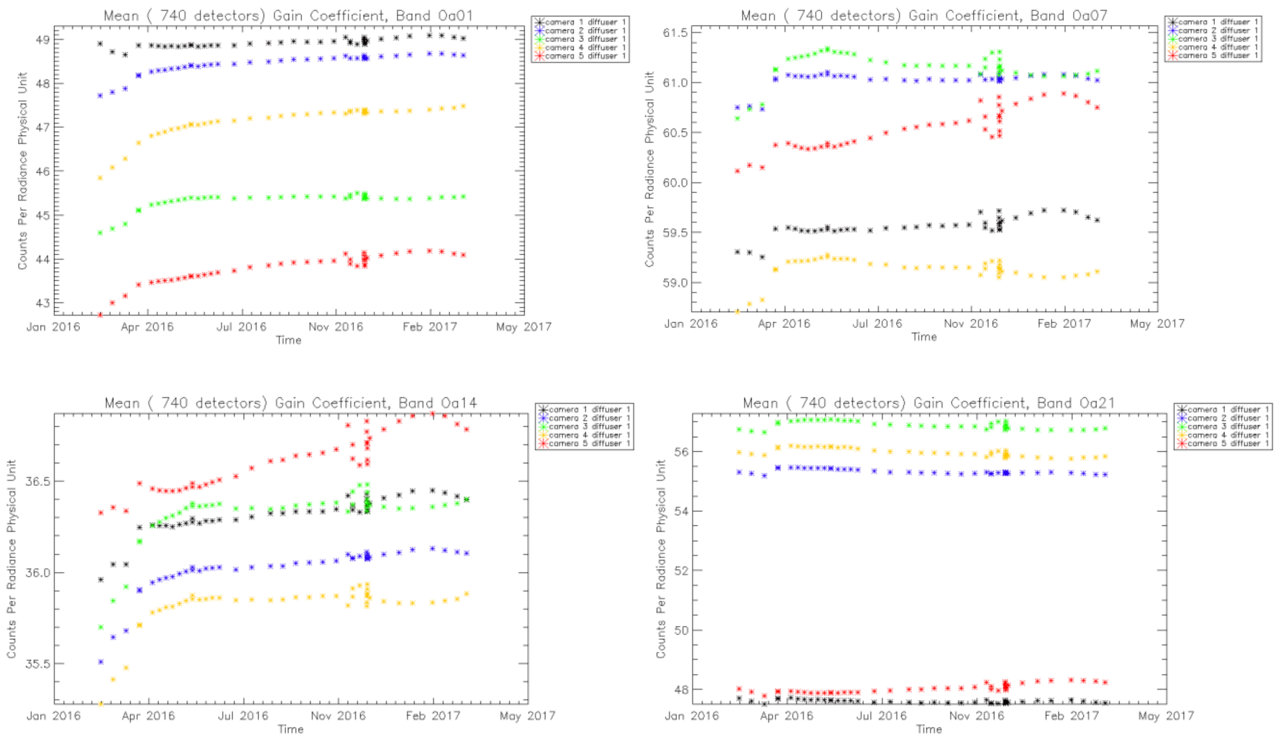

Figure 10: time evolution of the camera-averaged Absolute gain coefficients for bands Oa1, Oa7, Oa14 and Oa21 (from left to right and top to bottom).

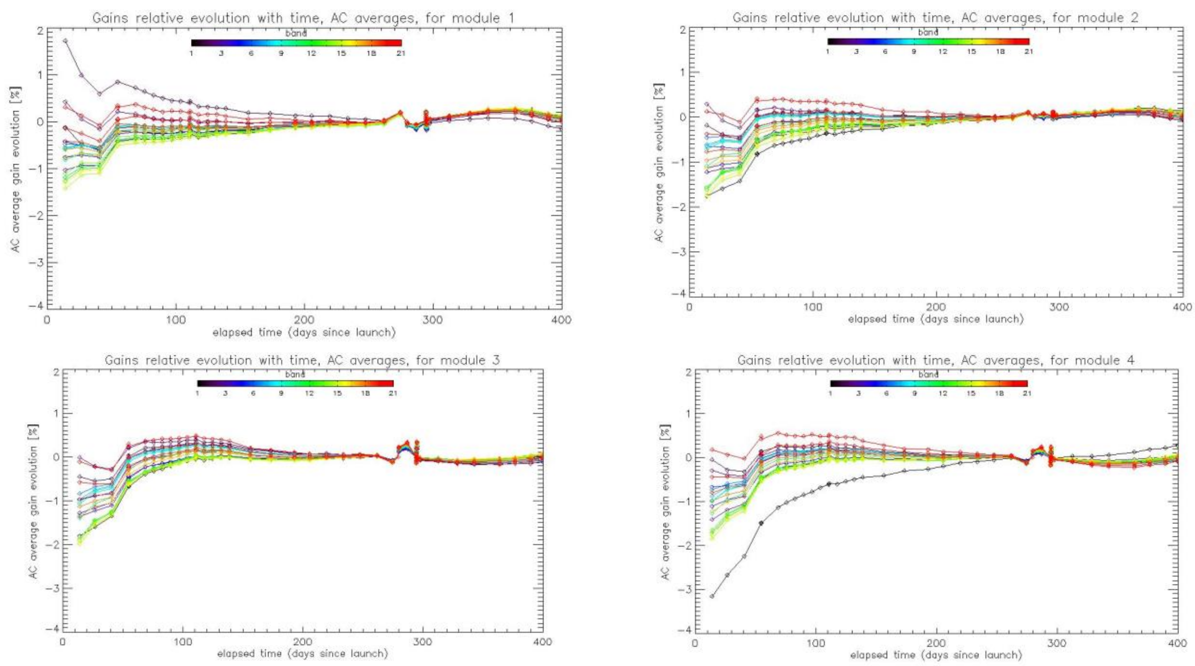

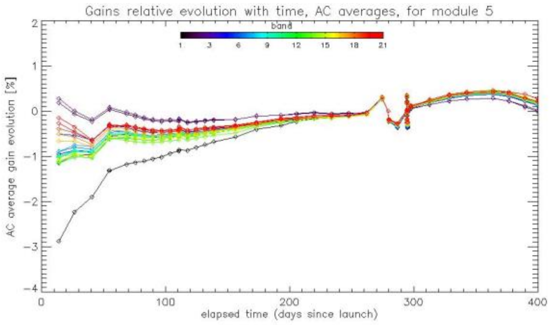

Figure 11: camera averaged gain relative evolution with respect to "best geometry" calibration (22/11), as a function of elapsed time since first calibration acquired after the fix of the Start Trackers issue; one curve for each band (see colour code on plots), one plot for each module.

Figure 12 further explore the geometry dependency at short and large time distances, selecting as reference the geometry that best match that of the BRDF modelling lowest residuals. Last two S01 calibrations (current cycle) as well past ones with about the opposite SAA differences are compared against the chosen reference (22/11). The impact is clearly seen, with a significant SAA dependent evolution that can be seen globally as a "white" curvature of the AC profile, increasing with azimuth difference, and with opposite curvature according to the sign of the azimuth difference. On the other hand, the instrument evolution is also clearly visible comparing ratios at symmetrical SAA differences but time lags with opposite signs (top-left with bottom right, top right with bottom left and to a lesser extent top right with centre left panes).

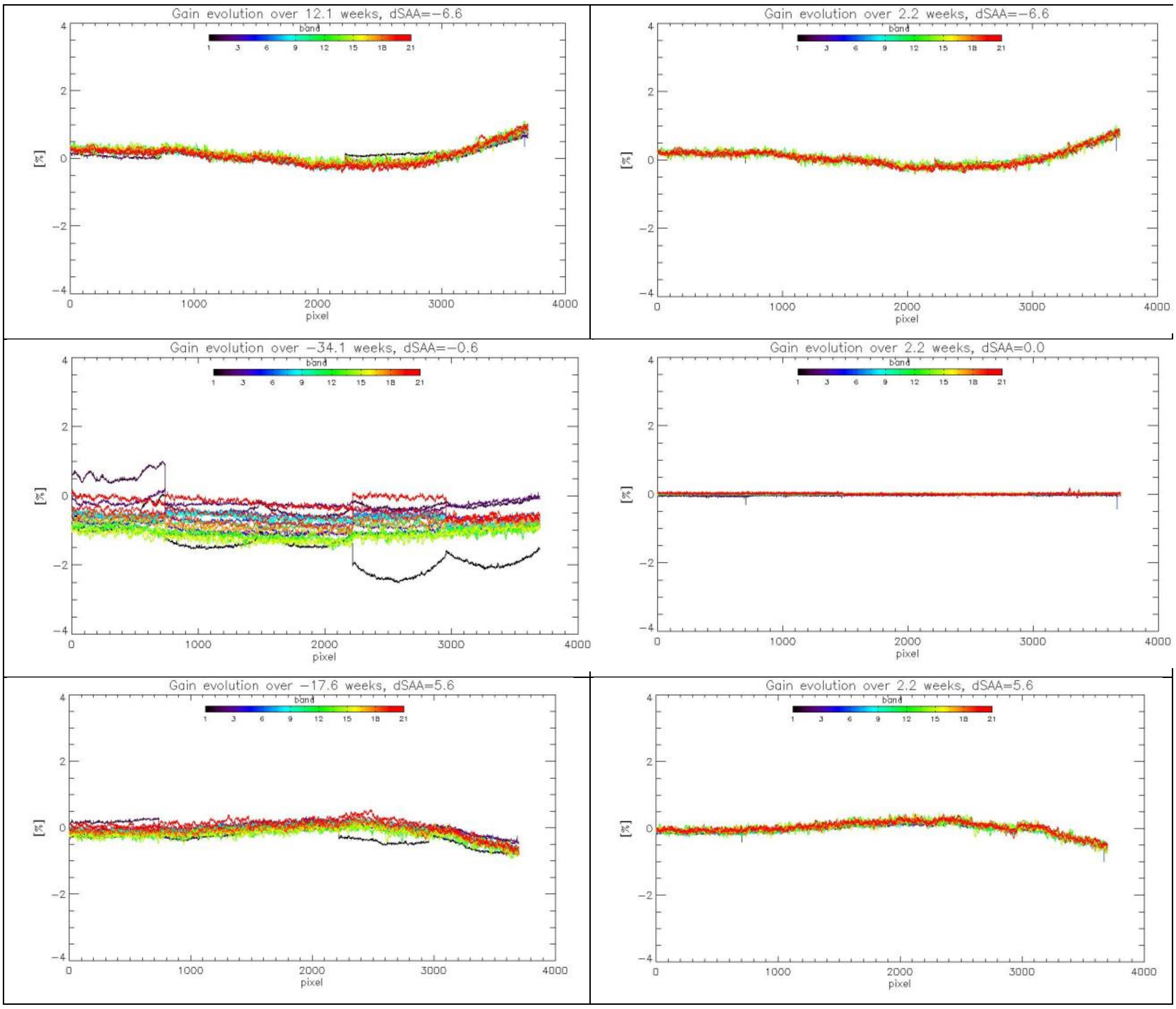

Figure 12: Across-track profiles of Gains relative evolution with respect to "best geometry" calibration over a relatively large time distance (from -34 to +12 weeks) and for varying geometries, more or less symmetrical with respect to reference one: on the right column time distance remains almost constant around 2 weeks, as calibrations compared to reference are selected within the Yaw Manoeuvres with SAA differences of -6.6, 0 and 5.6 degrees from top to bottom, while the left column show the comparisons at equal or close δSAA but as large as possible time distance.(from top to bottom time differences are respectively +12,-34 and -18 weeks). Influence of geometry and time are both clearly visible and can be distinguished from each other.

In order to get rid of the white variability (not spectrally dependant) caused by the BRDF model, all bands are normalized by band Oa18. Oa18 was chosen because NIR degrades slowest and because Oa20 and Oa21 are subject to Periodic Noise, e- leaks, etc … Results are presented Figure 13.

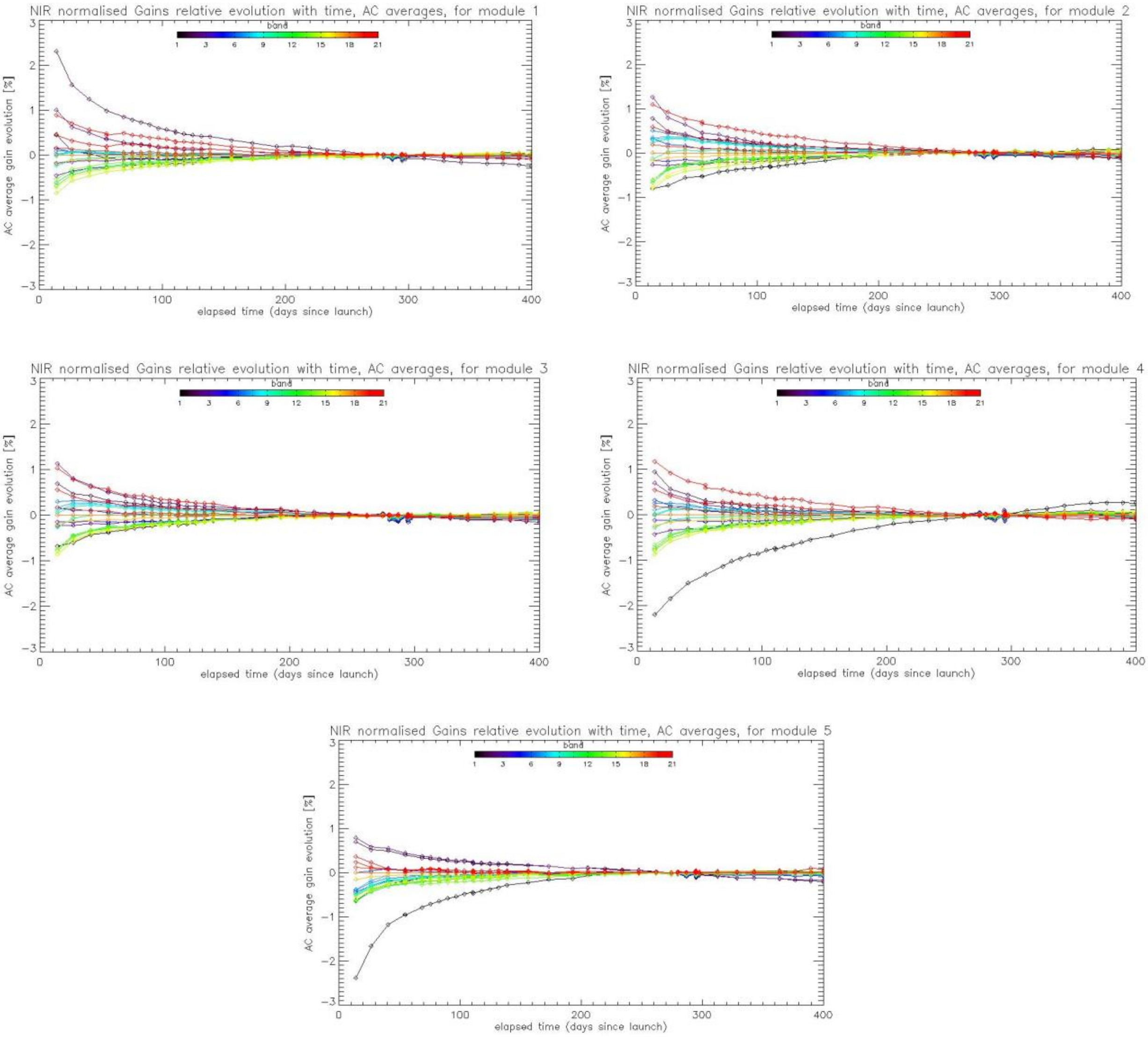

Figure 13: same as Figure 11 after normalization by band Oa18.

In Figure 13, we see that the ugly oscillations of Figure 11 have disappeared. However it is still surprising that some bands show an increase of sensitivity with time, while a decrease is expected since we are monitoring a 'degradation' of the instrument. Using the diffuser 2 results, we can say that this sensitivity increase cannot be explained by the ageing of diffuser 1. Moreover, we have checked that the spectral assignment drift cannot explain either this increase of sensitivity. Figure 14, compared to Figure 12, allows verifying the performance of the BRDF error correction on AC profiles.

Thus there is still something that remains unexplained concerning the evolution of the sensitivity of the instrument. Investigations are on-going.

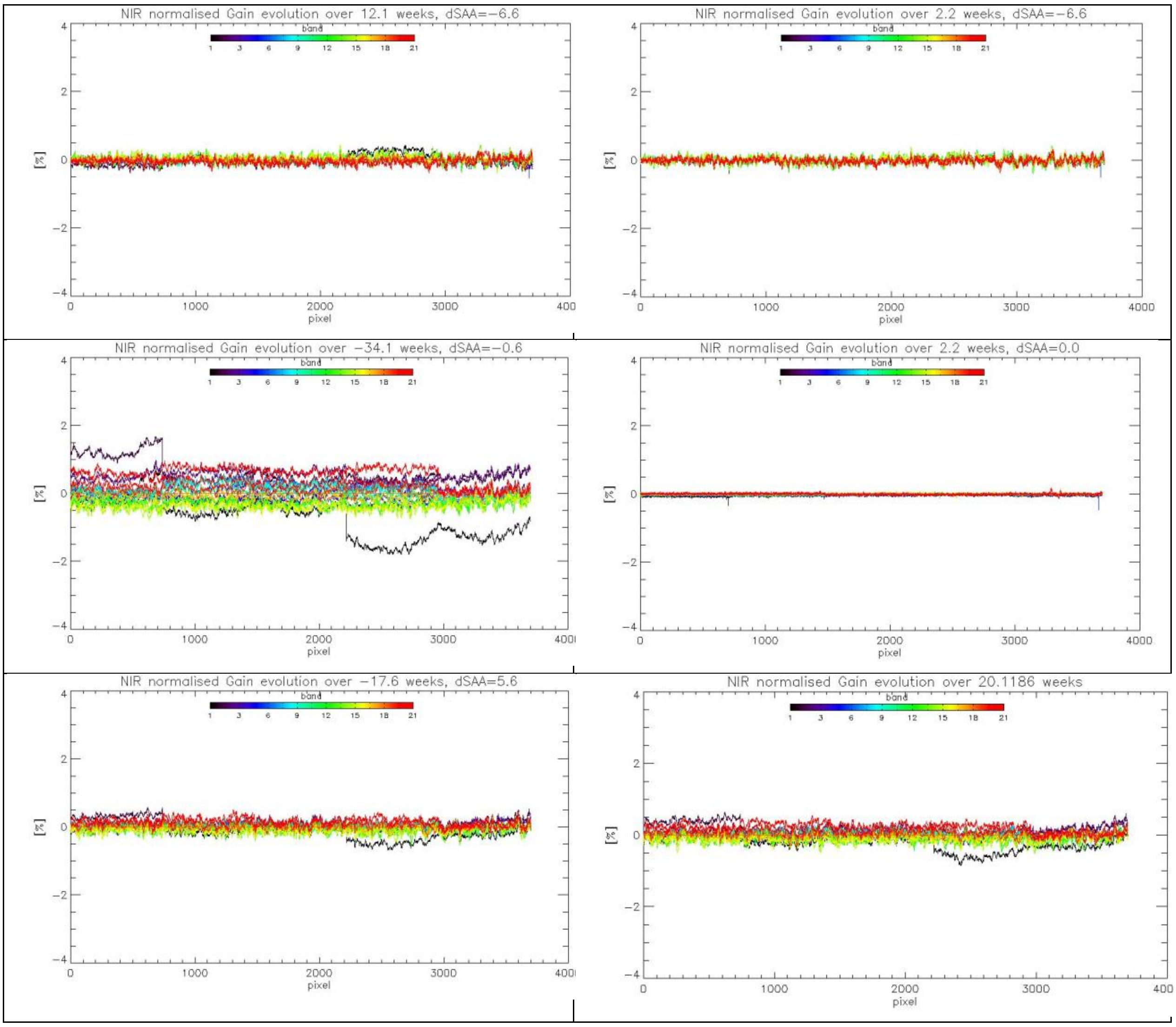

Figure 14: same as Figure 12 after normalization by band Oa18.

The time elapsed until the beginning of the mission is still too small to be able derive a degradation model, but Yaw Manoeuvres allow a direct quantification of the instrument sensitivity evolution between pairs of calibration with identical or close to identical geometries. This work is still on-going and will be presented in a future Cyclic Report.

1.2.3 Ageing of nominal diffuser [OLCI-L1B-CV-240]

There has been no calibration sequence S05 (reference diffuser) acquisition during cycle 015.

Consequently the last updated results are still valid and reported below.

The diffuser 1 Ageing is computed for each 3700 detector and each spectral band by formula:

Ageing(orb)=G1(orb_ref)/G2(orb_ref)- G1(orb_ref)/G2(orb_ref)

Where:

- G1 is the diffuser 1 (= nominal diffuser) Gain coefficients.
- G2 is the diffuser 2 (= reference diffuser) Gain coefficients
- orb_ref is a reference orbit chosen at the beginning of the mission

Ageing is represented in Figure 15 for band Oa1 and in Figure 16 for band Oa16

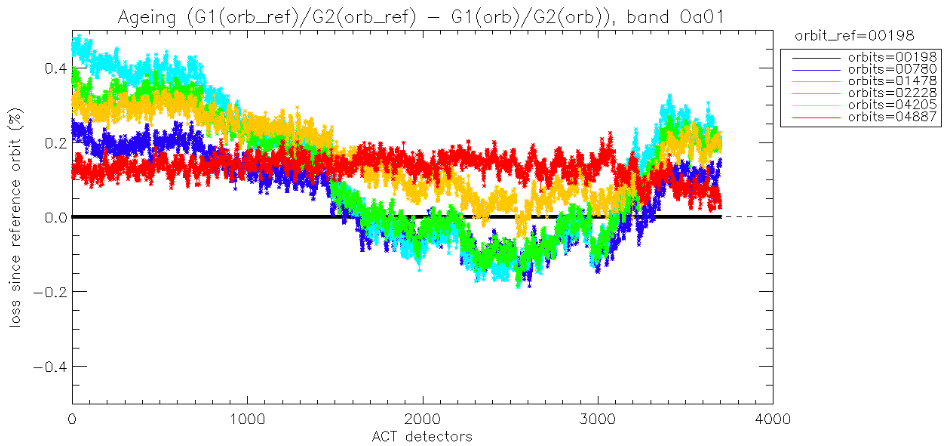

Figure 15: diffuser 1 ageing for spectral band Oa01. We see strong ACT low frequency structures that are due to residual of bad BRDF modelling.

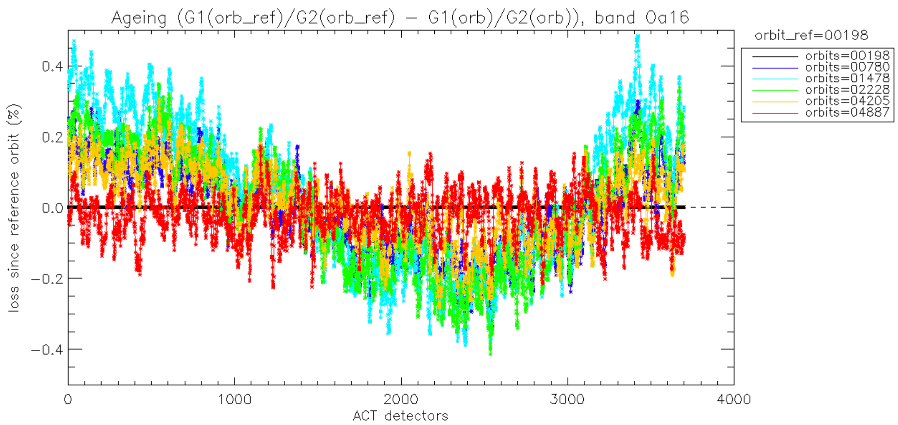

Figure 16: same as Figure 15 for spectral band Oa16. We use this band in order to normalize other bands and remove the ACT structures due to residual of bad BRDF modelling. Normalized curve for spectral band Oa01 is presented in Figure 17.

Figure 15 and Figure 16 show that the Ageing curves are impacted by a strong ACT pattern which is due to residuals of the bad modelling of the diffuser BRDF. This pattern is dependant of the azimuth angle. It is a 'white' pattern which means it is the same for all spectral bands. As such, we can remove this pattern by normalizing the ageing of all bands by the curve of band Oa16 which is expected not to be impacted by ageing because in the red part of the spectrum. We use an ACT smoothed version (window of 100 detectors) of band Oa16 in order to reduce the high frequency noise. Normalized ageing for spectral band Oa01 is represented in Figure 17 where we can see that this band is impacted by ageing of the diffuser.

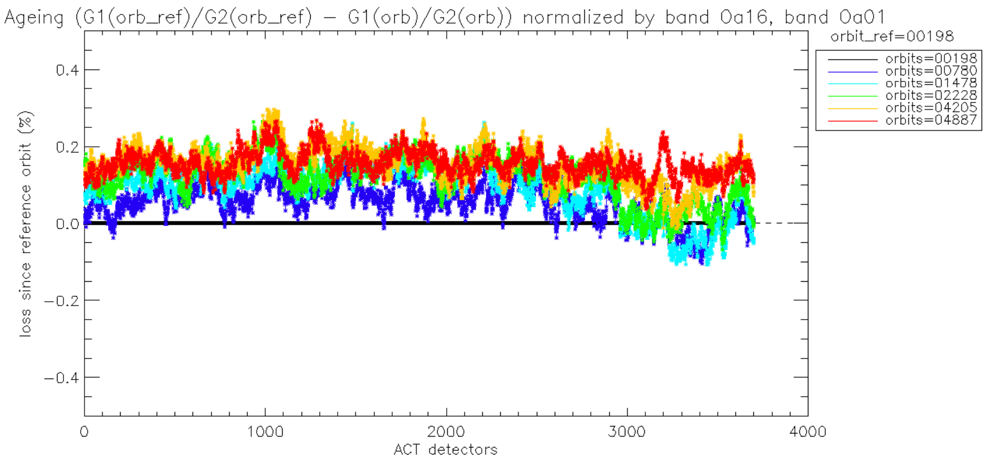

Figure 17: same as Figure 15 after normalization by band Oa16. Ageing of the diffuser 1 is now visible in the 5 cameras.

Camera averaged ageing (normalized by band Oa16) as a function of wavelength is represented in Figure 18 where we can see that ageing is stronger in the 'blue' (short wavelengths). Ageing is visible only for the 5 first spectral bands so far in the OLCI mission life.

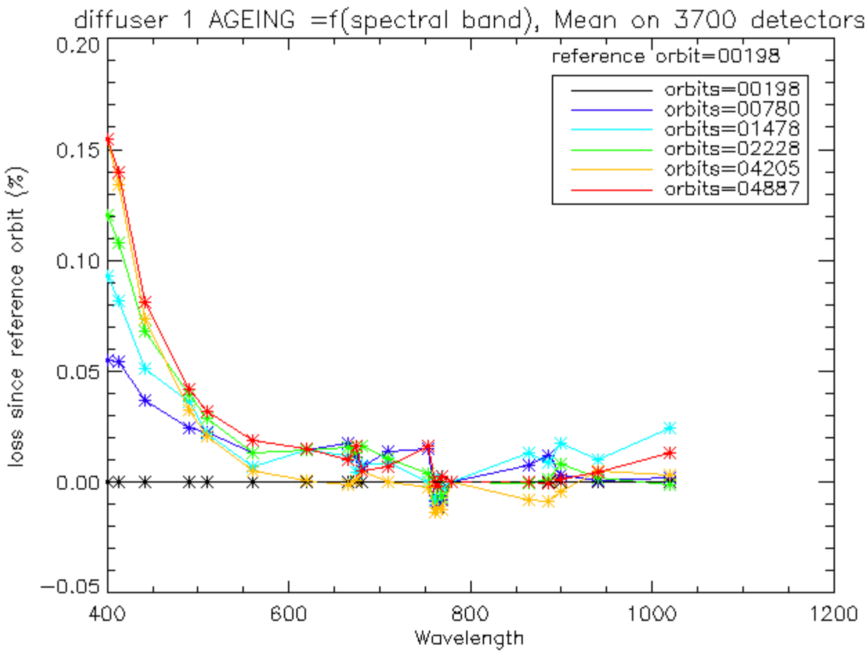

Figure 18: Diffuser 1 ageing as a function of wavelength (or spectral band). Ageing is visible in spectral band #1 to #5.

Figure 19 shows the evolution of the 5 camera averaged ageing as a function of time.

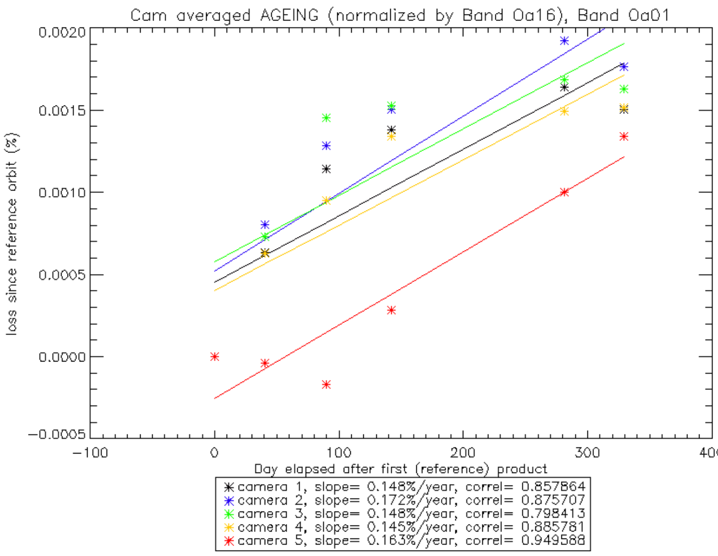

Figure 19: Camera averaged ageing (normalized by band Oa16) as a function of time. Linear fit for each camera is plotted. The slope (% loss per year) and the correlation coefficient of the linear fits are written in the legend at the bottom.

1.2.4 Updating of calibration ADF [OLCI-L1B-CV-260]

A number of OL_1_CAL_AX have been generated during cycle 015, to complete the set generated for the purpose of the S3VT reprocessing (see Cyclic Report of cycle 11). These OL_1_CAL_AX are modified with respect to the current baseline, as for the previous set, as follows:

1. A unique set of radiometric gains for all, based on “best available inflight geometry”, identified as the S01 sequence of 22/11/2016

2. Frequent update of the Dark Offset and Dark Current LUTs to minimise the impact of Periodic Noise: all calibrations with OCL ON have been selected, except those too close to their immediate predecessor (in practice this eliminates mostly the S05 of ageing sequences, 1 orbit later than S04 or S01). Validity dates have been set starting from the used calibration sequence and ending at next selected one, i.e. without any overlap.

The list of generated ADFs is:

S3A_OL_1_CAL_AX_20161225T084146_20170110T082623_20170329T153956__________________MPC_O_AL_R01.SEN3
S3A_OL_1_CAL_AX_20170110T082623_20170124T122451_20170329T153956__________________MPC_O_AL_R01.SEN3
S3A_OL_1_CAL_AX_20170124T122451_20170214T145948_20170329T153956__________________MPC_O_AL_R01.SEN3
S3A_OL_1_CAL_AX_20170214T145948_20170227T123949_20170329T153956__________________MPC_O_AL_R01.SEN3
S3A_OL_1_CAL_AX_20170227T123949_20170312T083848_20170329T153956__________________MPC_O_AL_R01.SEN3
S3A_OL_1_CAL_AX_20170312T083848_20170322T142139_20170329T153956__________________MPC_O_AL_R01.SEN3
S3A_OL_1_CAL_AX_20170322T142139_20991231T235959_20170329T153956__________________MPC_O_AL_R01.SEN3

The last one is intended to be used for NRT processing, with a different referencing:

S3A_OL_1_CAL_AX_20170322T142139_20991231T235959_20170329T153956__________________MPC_O_AL_014.SEN3

1.2.5 Radiometric Calibrations for sun azimuth angle dependency and Yaw Manoeuvres for Solar Diffuser on-orbit re-characterization [OLCI-L1B-CV-270 and OLCI-L1B-CV-280]

The Yaw Maneuver (YM) data consist in a set or radiometric calibrations acquired on the same day, hence without significant evolution of the instrument response, but at various SAA covering the yearly range. They represent as such a reference data set allowing assessing the instrument evolution, as well as for the derivation of an improved diffuser BRDF model as providing a complement to the on-ground characterization. EUMETSAT has put in place a dedicated study on the BRDF model improvement with the help of a sub-contracted consultant. S3-MPC OLCI L1 ESL leader has been asked to provide support as appropriate. This support to EUMETSAT BRDF modelling study has been continuously provided through data provision, technical support and participation to technical meetings.

The validation methodology for the updated diffuser BRDF model has been defined by the OLCI L1 ESL, through the comparison of its ability to recover the instrument evolution with respect to the reference derived using equal-SAA calibrations (from YM data paired to nominal attitude at various dates). This methodology has been applied to the first test model. The validation methodology is further detailed in the following three steps:

- the YM day data set provides a set of calibrations covering the yearly SAA range without significant evolution of the instrument sensitivity; these can be paired with calibrations spread over the mission with equal or almost equal SAAs, each pair providing a measure of the instrument evolution without any residual SAA dependency, considered as the reference;

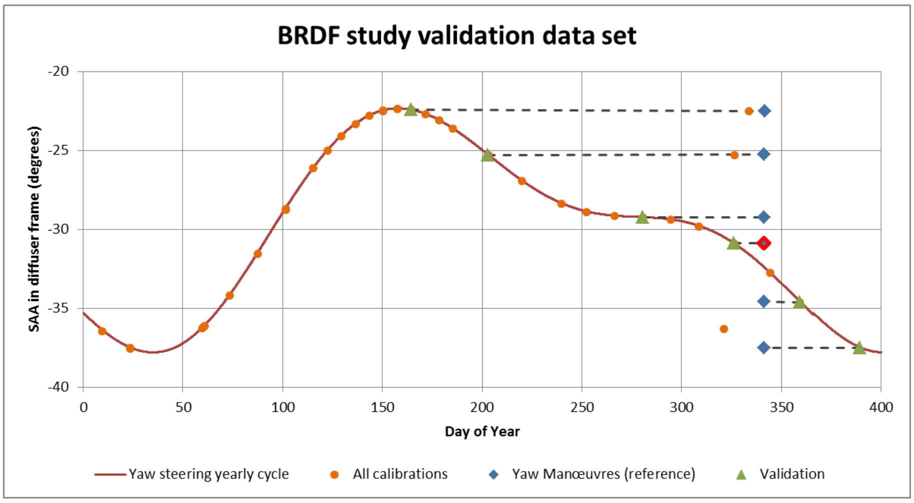

Figure 20: nominal SAA yearly cycle (red solid line) with all acquired calibrations (orange circles, note that the first 2 are actually early 2017 calibrations), and highlighted Yaw Manoeuvre's ones (blue diamonds, among which the reference geometry is framed in red) and corresponding test data set at equal SAA (green triangles).

- in parallel, the same set of test calibrations (green triangles in Figure 20) can be compared with a unique YM day calibration (red framed diamond) in order to highlight the current BRDF model dependency with SAA;
- step 2 is repeated using Gains computed with the updated BRDF model and compared with results of steps 1 & 2.
- In addition, it is verified that the updated BRDF model does not significantly change the absolute gains at the reference geometry, the in-flight one that best match one of the ground characterisation illumination conditions (Figure 21).

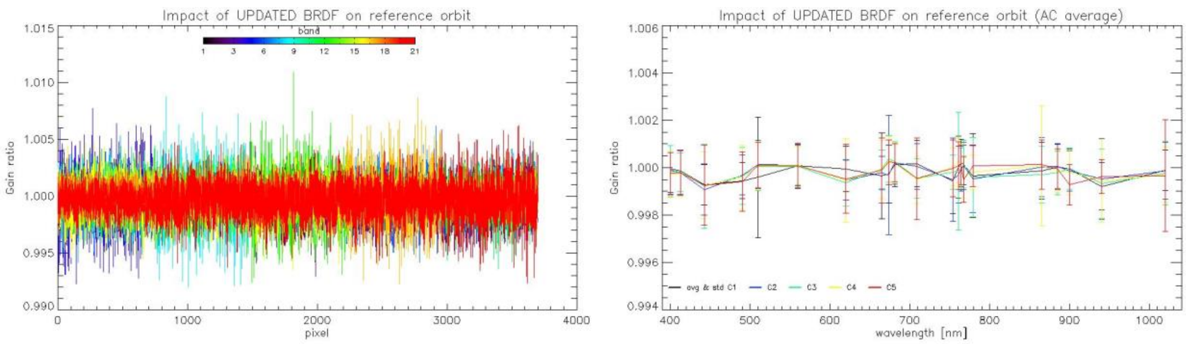

Figure 21: gain ratios at reference geometry, updated BRDF model over nominal one, as cross-track profiles for all bands (left), and as AC averages within each camera vs. wavelengths (right), allow to verify that the updated BRDF model do not significantly change the absolute radiometric calibration.

Examples are provided below (Figure 22 to Figure 24)showing that the updated BRDF model allows retrieving correctly the instrument evolution, without the dependency to SAA, but at the cost of additional noise, likely introduced by the per-pixel modelling. Action is in place at EUMETSAT, with S3-MPC support, to explore the possibilities of noise reduction in modelling methodology.

Oa1	Oa5

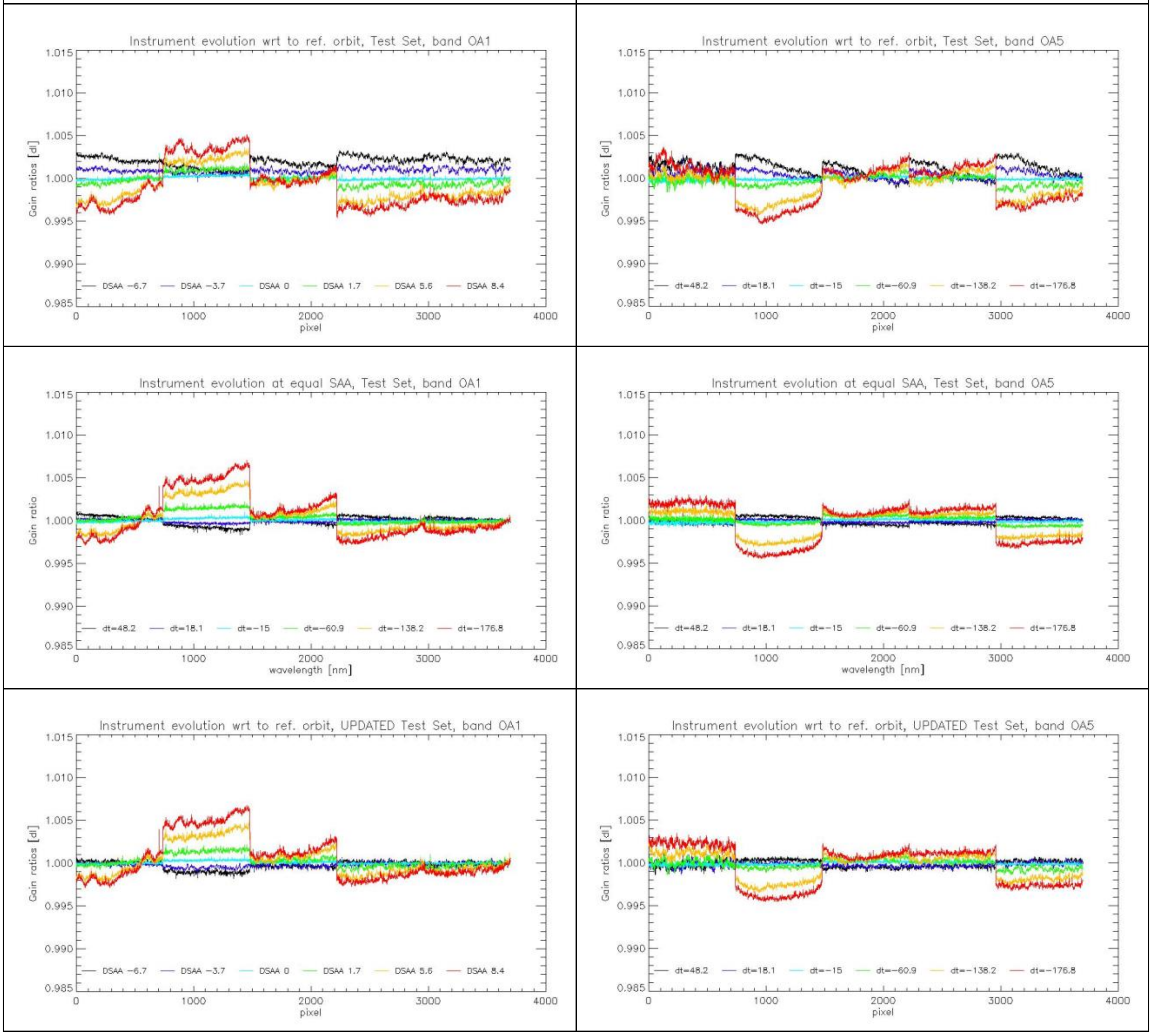

Figure 22: Instrument evolution for Oa1 & Oa5 (400 & 510 nm) as a function of pixels (all cameras side-by-side) and as derived using: nominal BRDF model at various SAA against a single YM reference (top), nominal BRDF model at various SAA against matching SAA YM reference (centre), and using UPDATED BRDF model at various SAA against a single YM reference (bottom).

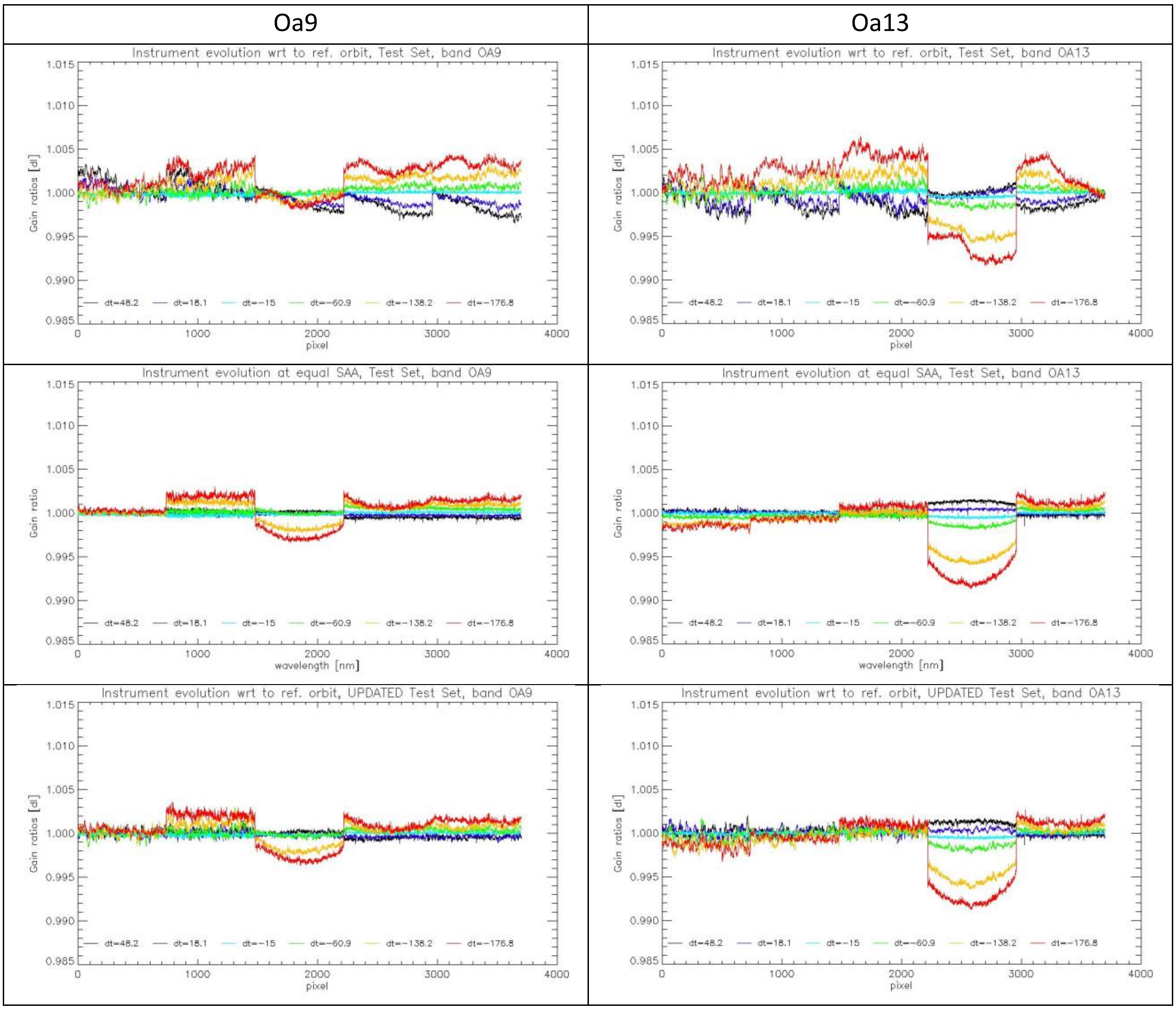

Figure 23: Same as Figure 22 for Oa9 and Oa13 (674 & 761 nm).

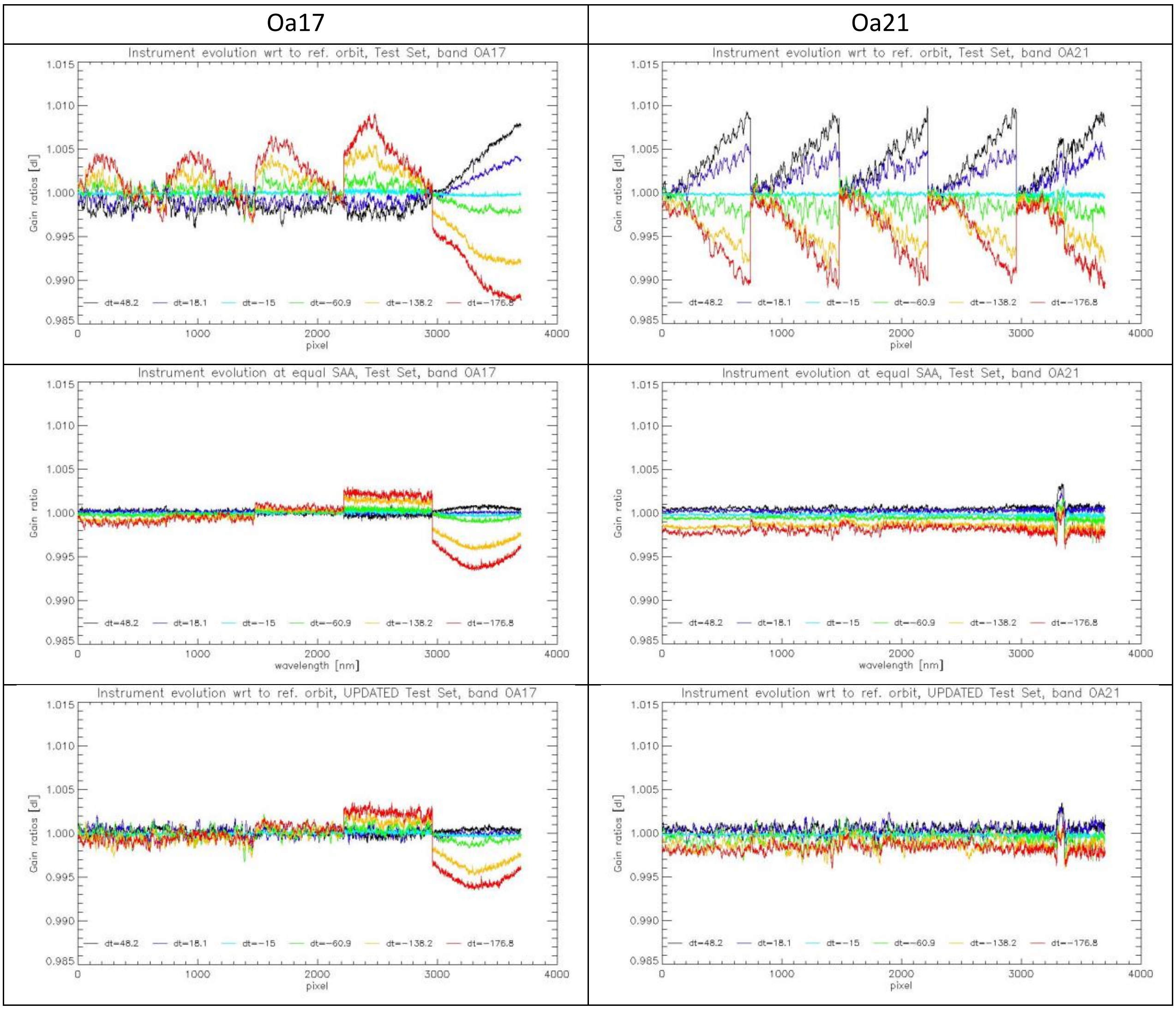

Figure 24: Same as Figure 22 for Oa17 and Oa21 (865 & 1020 nm).

1.3 Spectral Calibration [OLCI-L1B-CV-400]

There has been no Spectral Calibration acquisition during cycle 015.

1.4 Signal to Noise assessment [OLCI-L1B-CV-620]

1.4.1 SNR from Radiometric calibration data.

SNR computed for all calibration data as a function of band number is presented in Figure 25.

SNR computed for all calibration data as a function of orbit number for band Oa01 (the less stable band) is presented in Figure 26.

There is no significant evolution of this parameter during the current cycle and the ESA requirement is fulfilled for all bands.

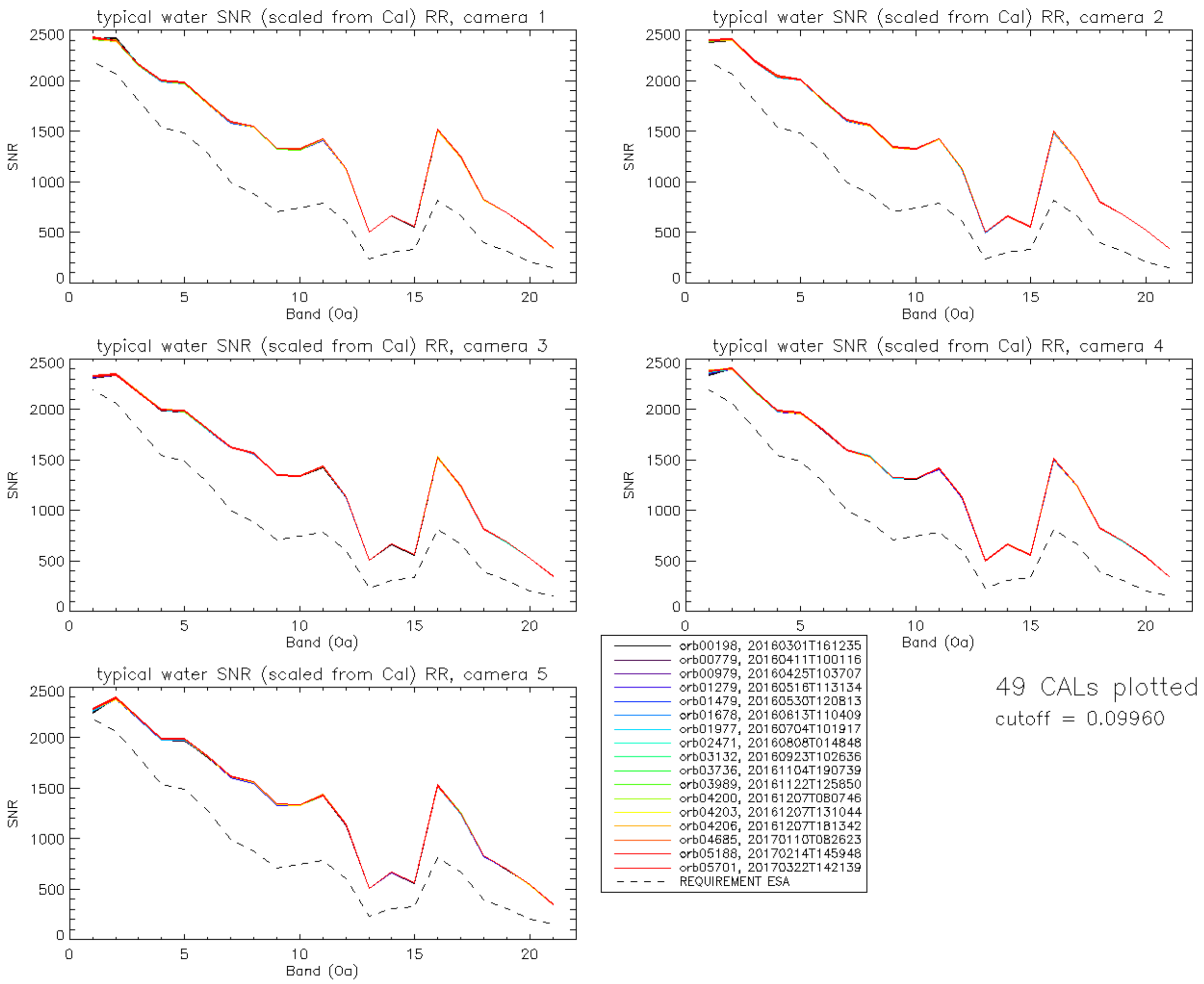

Figure 25: Signal to Noise ratio as a function of the spectral band for the 5 cameras. These results have been computed from radiometric calibration data. All calibrations except first one (orbit 183) are presents with the colours corresponding to the orbit number (see legend). The SNR is very stable with time: the curves for all orbits are almost superimposed. The dashed curve is the ESA requirement.

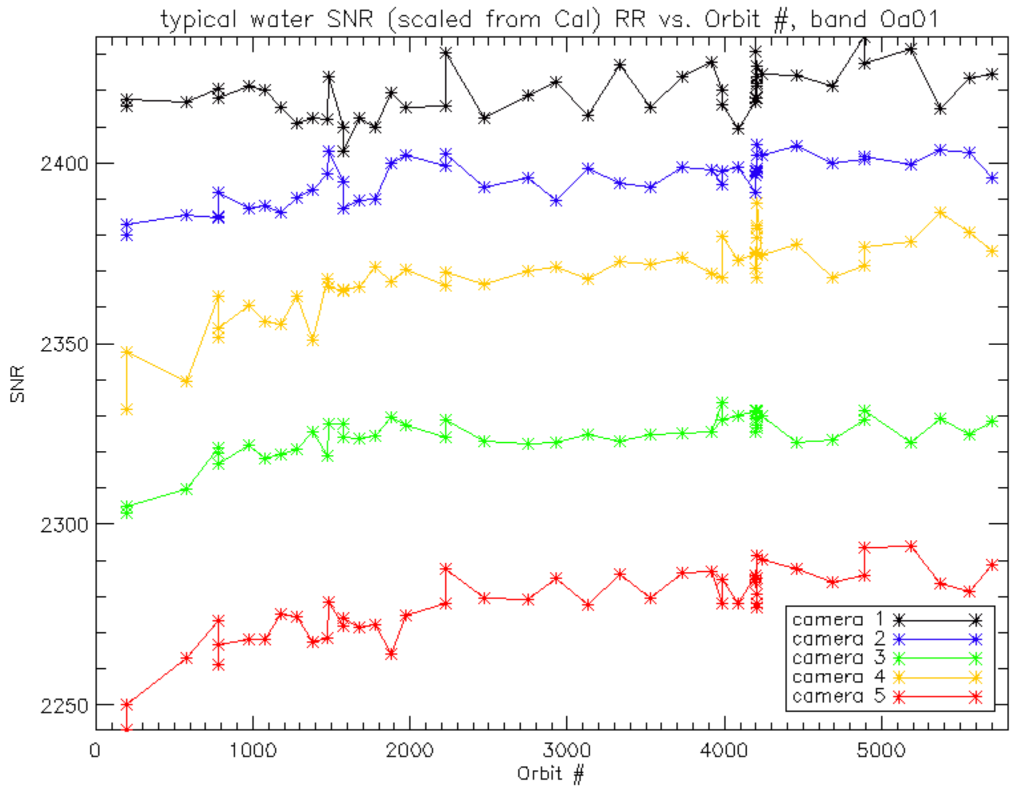

Figure 26: long-term stability of the SNR estimates from Calibration data, example of channel Oa1.

1.4.2 SNR from EO data.

There has been no update on SNR assessment from EO data during the cycle. Last figures (cycle 9) are considered valid.

1.5 Geometric Calibration/Validation

- There has been no update on Geometric Calibration quantitative assessment during the cycle. Last figures (cycle 10) are considered valid.
- Qualitative assessment by product inspection showed no detectable performance evolution.

2 OLCI Level 1 Product validation

[OLCI-L1B-CV-300], [OLCI-L1B-CV-310] – Radiometric Validation

S3ETRAC Service

Activities done

The S3ETRAC service extracts OLCI L1 RR and SLSTR L1 RBT data and computes associated statistics over 49 sites corresponding to different surface types (desert, snow, ocean maximizing Rayleigh signal, ocean maximizing sunglint scattering and deep convective clouds). The S3ETRAC products available at ftp://ftp.acri-cwa.fr are used for the assessment and monitoring of the L1 radiometry (optical channels) by the ESLs.

Statistics on the number of S3ETRAC products generated approximatively at the end of Cycle 15 (end of March.):

	Cycle 14	Cycle 15	Increase since Cycle N-1	
OLCI/DESERT	1118	1476	358	32%
OLCI/SNOW	257	267	10	4%
OLCI/RAYLEIGH	309	423	114	37%
OLCI/SUNGLINT	94	101	7	7%
OLCI/DCC	60	73	13	22%
Total OLCI	**1838**	**2340**	**502**	**27%**
SLSTR/DESERT	209	218	9	4%
SLSTR/SNOW	16	16	0	0%
SLSTR/RAYLEIGH	342	501	159	46%
SLSTR/SUNGLINT	62	80	18	29%
Total SLSTR	**629**	**815**	**186**	**30%**
TOTAL	**2467**	**3155**	**688**	**28%**

All details about the S3ETRAC/OLCI and S3ETRAC/SLSTR statistics are provided on the S3ETRAC website http://s3etrac.acri.fr/index.php?action=generalstatistics

- Number of OLCI products processed by the S3ETRAC service
- Statistics per type of target (DESERT, SNOW, RAYLEIGH, SUNGLINT and DCC)
- Statistics per sites
- Statistics on the number of records

For illustration, we provide below statistics on the number of S3ETRAC/OLCI records generated per type of targets (DESERT, SNOW, RAYLEIGH, SUNGLINT and DCC).

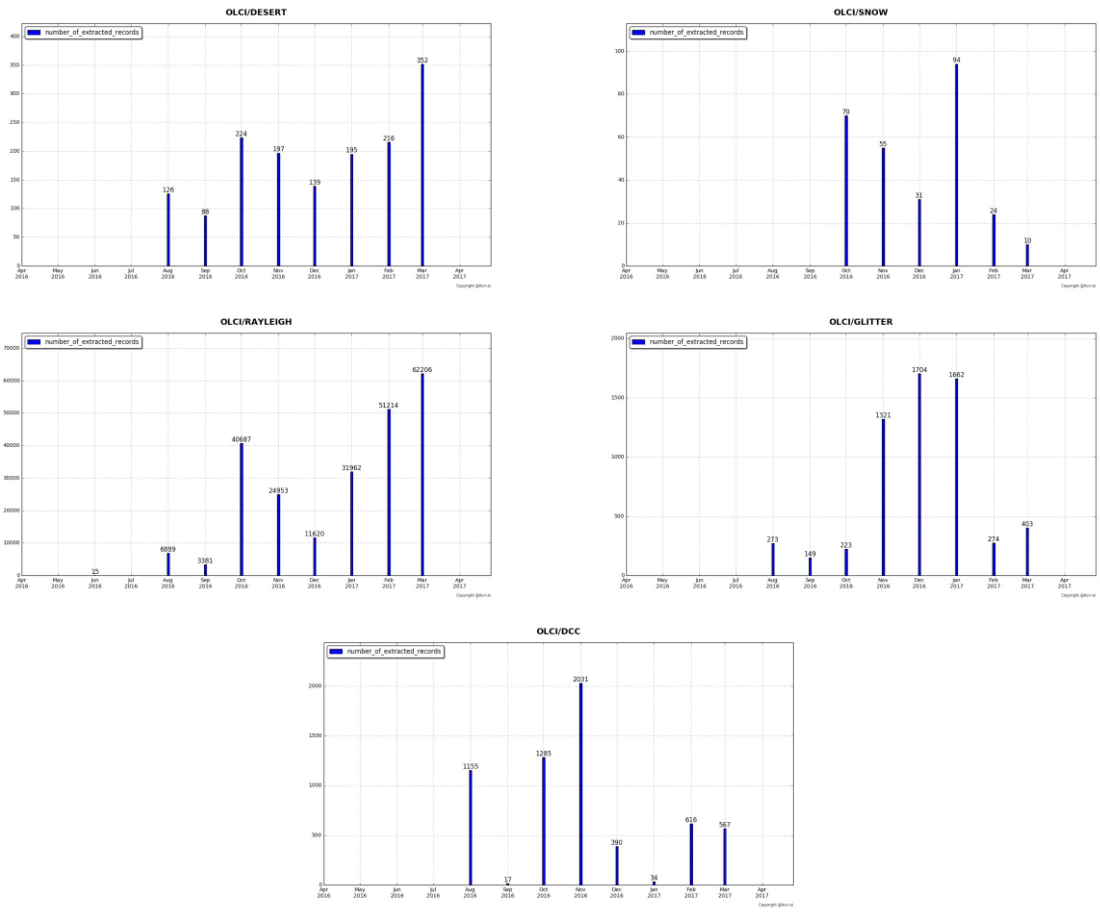

Figure 27: summary of S3ETRAC data extraction for OLCI (number of generated records for each month, one plot per site type).

<u>Radiometric validation with DIMITRI</u>

I-Validation over PICS

1. Downloading and ingestion of 65 L1B-LN1-NT products from PB-N02 over the 6 desert calval-sites (Algeria3 & 5, Libya 1 & 4 and Mauritania 1 & 2). Where the ingested time-series has been extended until 26th March 2017.

2. The results are consistent overall the six used PICS sites (Figure 28). OLCI reflectance shows strong fluctuation in the beginning of the commissioning phase (about ±8% amplitude) between March and July 2016. The temporal average over the period **September 2016 – March 2017** of the elementary ratios (observed reflectance to the simulated one) shows values within 2% (mission requirements) over all the VNIR bands (Figure 29). The spectral bands with significant absorption from water vapor and O_2 (Oa11, Oa13 and Oa14) show an outlier ratio.

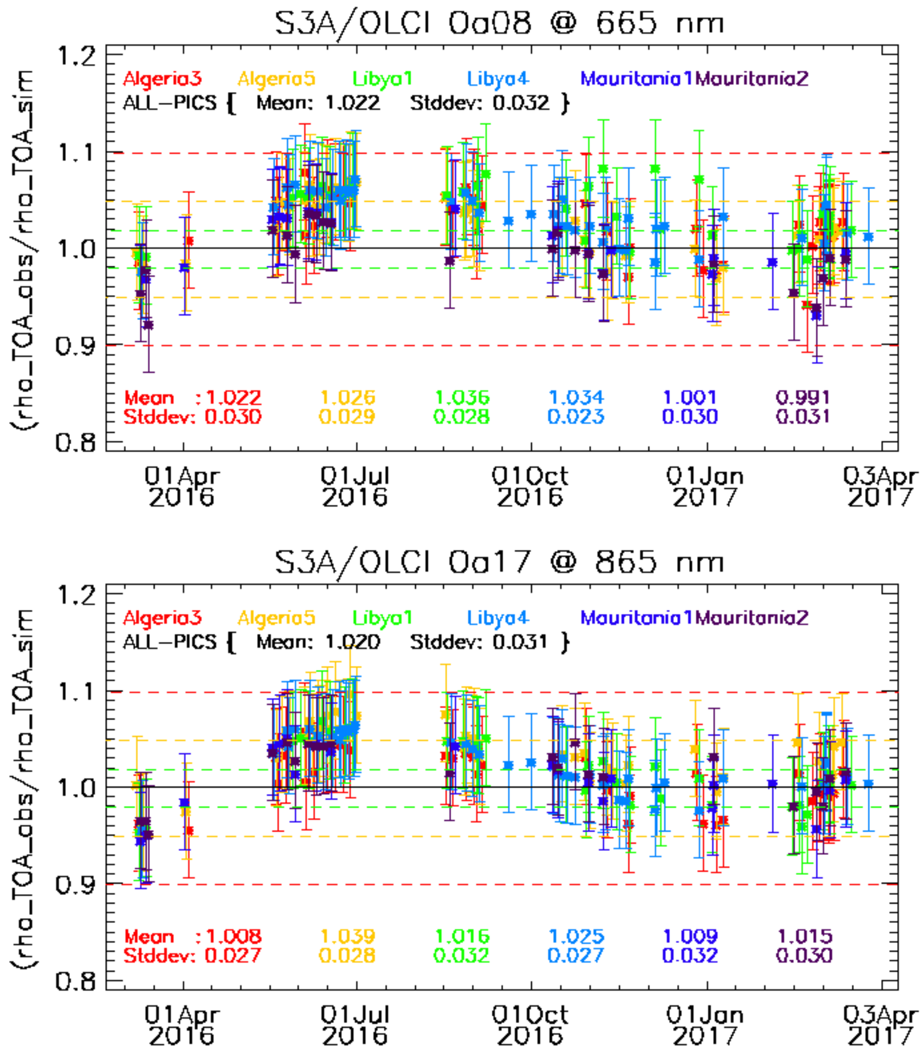

Figure 28: Time-series of the elementary ratios (observed/simulated) signal from S3A/OLCI for (top) band Oa8 and (bottom) band Oa17 over Six PICS Cal/Val sites. Dashed-green, orange and red lines indicate the 2%, 5% and 10% respectively. Error bars indicate the desert methodology uncertainty.

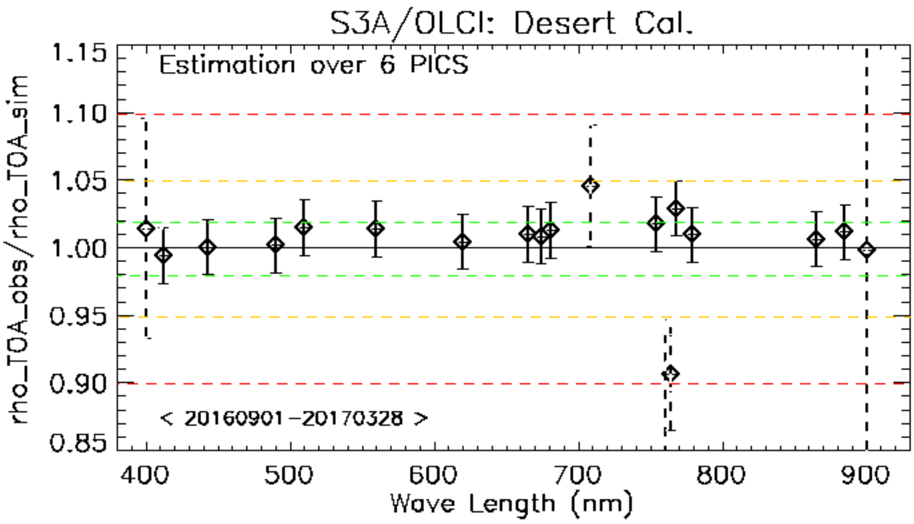

Figure 29: The estimated gain values for S3A/OLCI over the 6 PICS sites identified by CEOS over the period September 2016 – March 2017 as a function of wavelength. Dashed-green, orange and red lines indicate the 2%, 5% and 10% respectively. Error bars indicate the desert methodology uncertainty.

II-Intercomparison S3A/OLCI, S2A/MSI and LANDSAT/OLI over PICS

1. The reflectance time-series from MSI-L1C products, LANDSAT/OLI, Aqua/MODIS and OLCI-L1B products over PICS have been compared using PICS method. The ratios of the observed/simulated signals have been computed from the four sensors over **September 2016-March 2017** (Figure 30 and Figure 31). From November 2016 onward, the three sensors MODISA, MSI and OLCI show almost the same reflectance evolution.

2. The temporal average of the relative gain coefficients of PICS method are summarized below on Figure 32. The results show that OLCI ratios over October-November are within the mission requirements (<2%) over the VNIR spectral range. Band Oa11 is outlier as for all the high gaseous absorption bands in DIMITRI. However, except Oa03 and Oa04, all the similar bands of OLCI, MSI and OLI show a very good agreement over the same acquisition period.

3. These results are very interesting, on the one hand they show the good agreement of OLCI with the other sensors from September 2016 onward, and on the other hand, they exhibit the high reflectance signal of OLCI during the first 6 months of the commissioning period. .

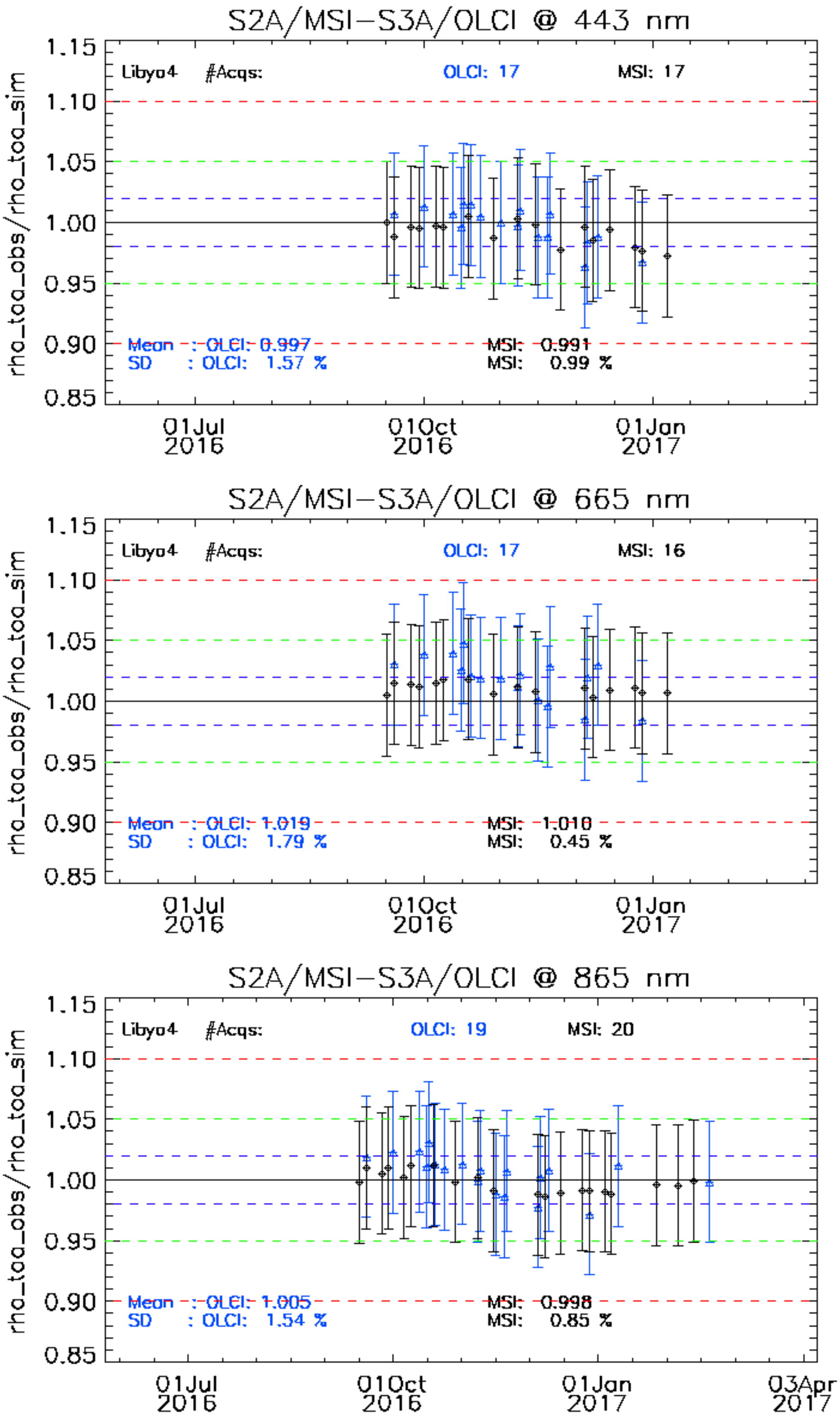

Figure 30: Time-series of the elementary ratios (observed/simulated) signal from (black) S2A/MSI and (blue) S3A/OLCI for bands (top to bottom) 443nm, 665nm and 865nm over Libya4 Cal/Val site. Dashed-blue, green and red lines indicate the 2%, 5% and 10% respectively. Error bars indicate the methodology uncertainty.

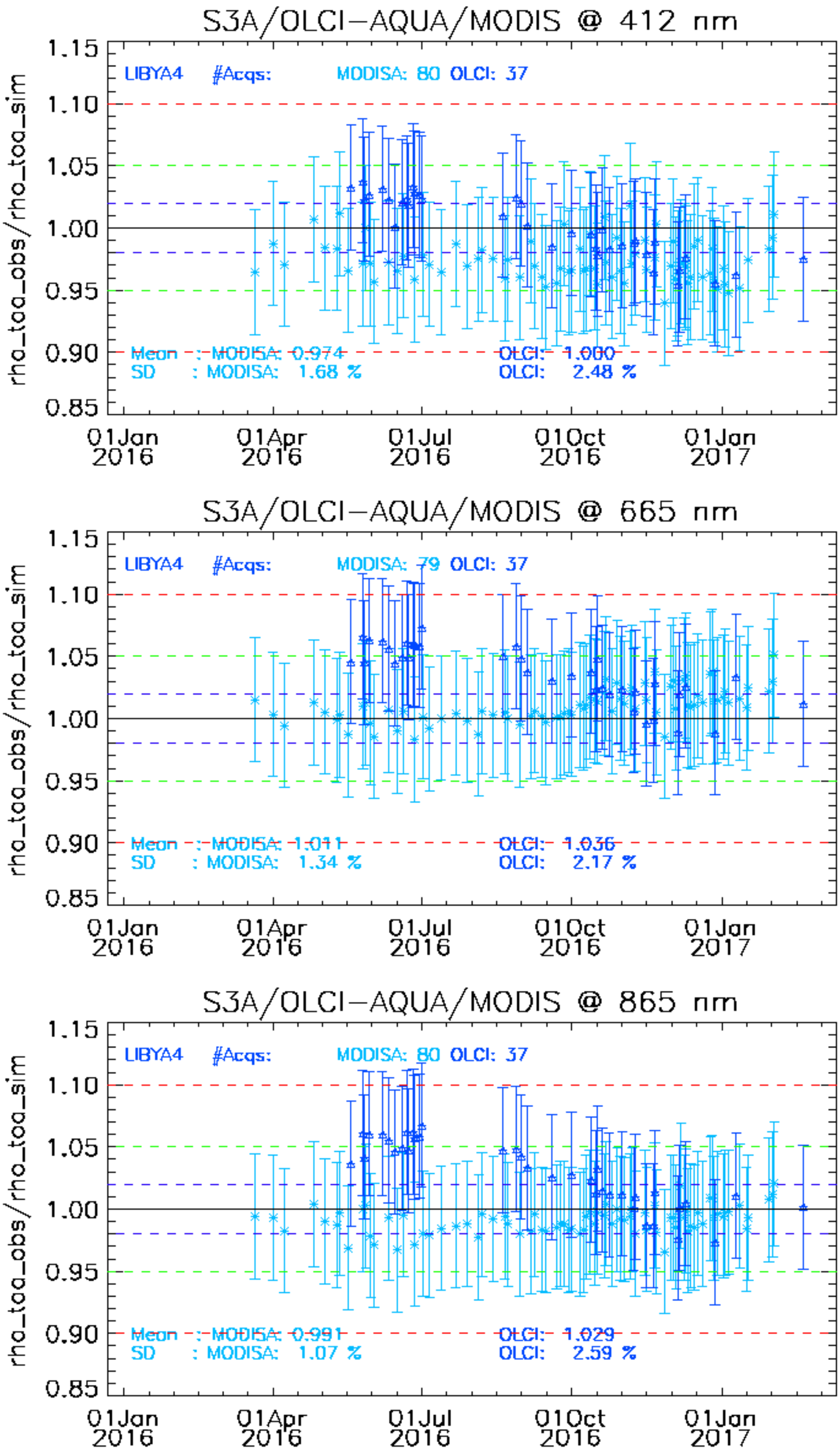

Figure 31: Time-series of the elementary ratios (observed/simulated) signal from (Cyan) Aqua/MODIS and (blue) S3A/OLCI for bands (top to bottom) 443nm, 665nm and 865nm over Libya4 Cal/Val site. Dashed-blue, green and red lines indicate the 2%, 5% and 10% respectively. Error bars indicate the methodology uncertainty.

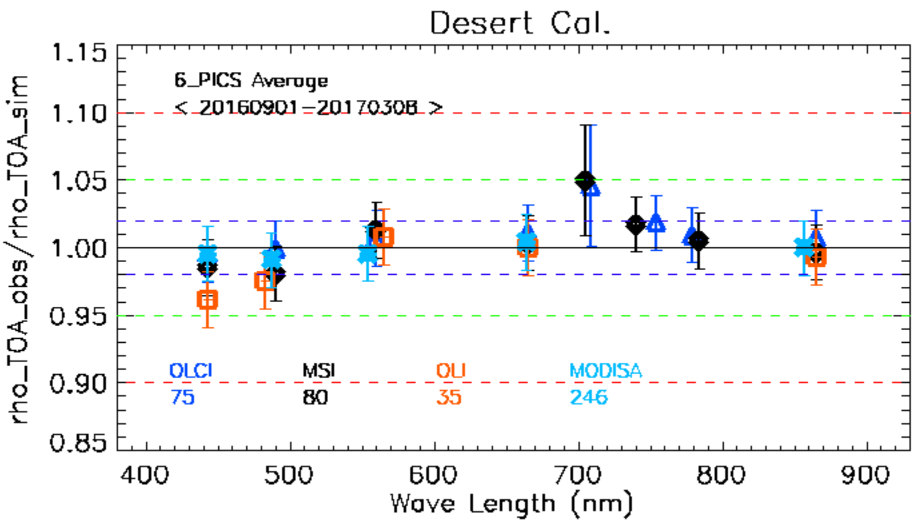

Figure 32: The estimated gain coefficients (observed/simulated signal) over the period September 2016 – March 2017 from (black) S2A/MSI, (blue) S3A/OLCI, (cyan) Aqua/MODIS and (orange) LANDSAT/OLI over the six Cal/Val-sites as a function of wavelength. Dashed-blue, green and red lines indicate the 2%, 5% and 10% respectively. Error bars indicate uncertainty associated to the estimated gain coefficients.

III-Validation over Rayleigh

The investigations of the discrepancy between the results from ARGANS and ESTEC, when both use the same CFI (DIMITRI), are done. Following to several email-exchange with Marc Bouvet (ESTEC) then personal meeting during the RadCalNet workshop, we found that ARGANS and ESTEC have used different thresholds over Rayleigh in DIMITRI. ARGANS's ESL has performed Rayleigh using ESTEC-thresholds over the period September 2016-March 2017. We found slightly different results due to the different period. The outcome of this analysis will be provided to the S3MPC in a separate TN soon.

During this period, we have ingested about 84 L1B products to DIMITRI and run Rayleigh. The results over this cycle are similar to the previous one over the period September 2016 – March 2017, which show a rather consistency with desert method over bands >500 nm. While bands Oa01-Oa05 display a bias values between 2%-5%, bands Oa6-Oa9 exhibit biases within 2% (mission requirements) (Figure 33).

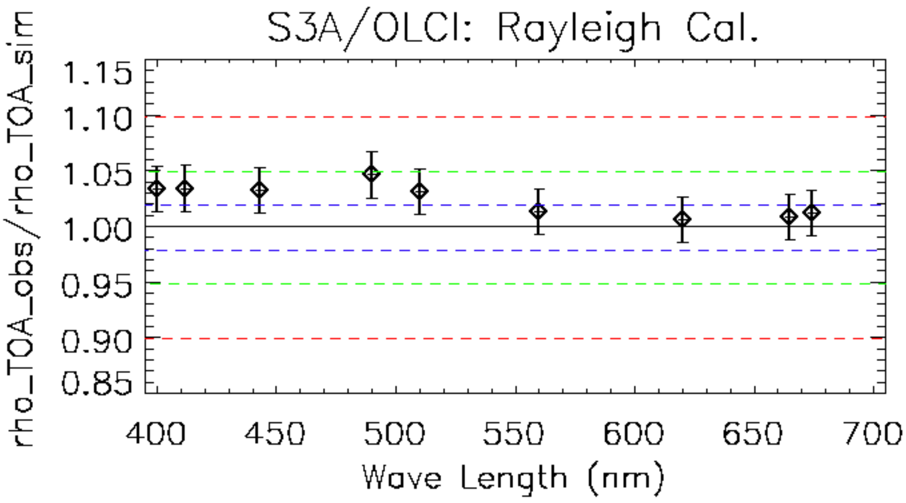

Figure 33: The estimated gain values for S3A/OLCI over the 4 Ocean (Atl-NW_Optimum, Atl-SW_Optimum, Pac-NE_Optimum and SIO_Optimum) over the period September 2016 – March 2017 as a function of wavelength. Dashed-blue, green, and red lines indicate the 2%, 5% and 10% respectively. Error bars indicate the methodology uncertainty.

As the S3ETRAC readers are fully developed now, we have ingested about 200 products. The radiometry seems correct over the 5 considered CalVal-sites, but the Cloudiness percentage (Cloud-Fractions) seems to be wrong in S3ETRAC products, which prevents Rayleigh method to run correctly. The investigation of this issue is on-going.

Radiometric validation with OSCAR

The S3ETRAC Rayleigh scenes of February 2017 over 2 sites (IndS and AtlN) have been processed, processing of other sites is on-going. Corresponding results are shown on Figure 34.

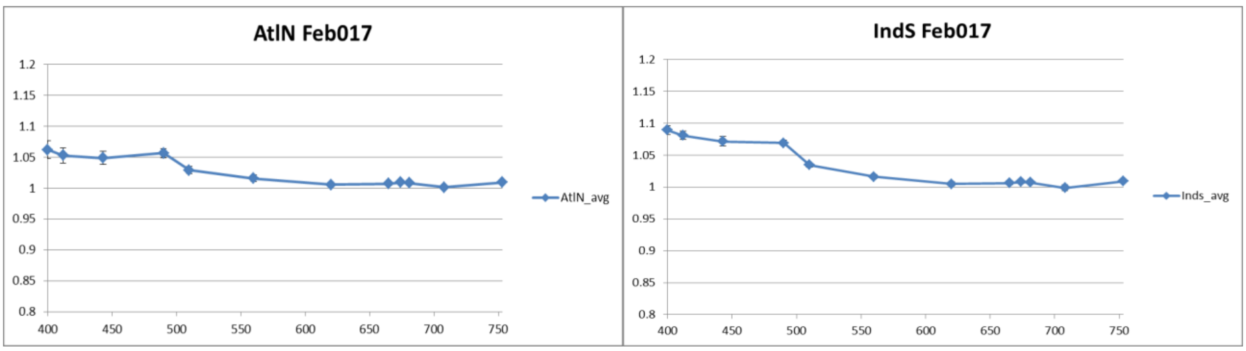

Figure 34 Oscar Rayleigh results for February 2017 for AtlN and IndS sites.

3 Level 2 Land products validation

[OLCI-L2LRF-CV-300]

There has been no update on Land products validation quantitative assessment during the cycle. Last figures (cycle 14) are considered valid.

Qualitative assessment by product inspection showed no detectable performance evolution.

[OLCI-L2LRF-CV-410 & OLCI-L2LRF-CV-420] – Cloud Masking & Surface Classification for Land Products

There has been no update on Land Cloud Masking & Surface Classification validation quantitative assessment during the cycle. Last figures (cycle 10) are considered valid.

Qualitative assessment by product inspection showed no detectable performance evolution.

Validation of Integrated Water Vapour over Land

Reprocessed as well as recently generated products have been analysed and compared with match-up data over Land. Validation data is provided by the SUOMI Net ground-based GNSS data set, mostly acquired over North America. 1702 matchups are available for the NRT/NTC dataset acquired in October and November 2016, 286 matchups are available for the Reprocessed dataset. The former is compared with FR data, the latter with both FR and RR.

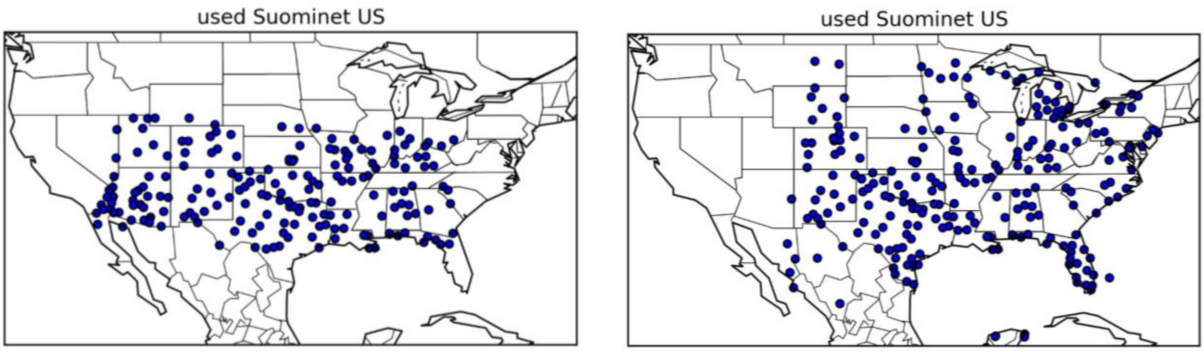

Figure 35: location of the SUOMI Net IWV matchups for the Oct/Nov NRT/NTC dataset (left) and the Reprocessed dataset (right).

Scatter plots of OLCI vs. in-situ data are presented below on Figure 36 for the NRT/NTC dataset and on Figure 37 for the Reprocessed dataset. Results are consistent for all datasets (NRT/NTC vs. reprocessed, FR vs. RR) and show a systematic overestimation of about 13% that requires further investigation. The RMS deviation is about 10%.

The cloud screening seems efficient for IWV retrieval as otherwise significant occurrence of underestimation should occur.

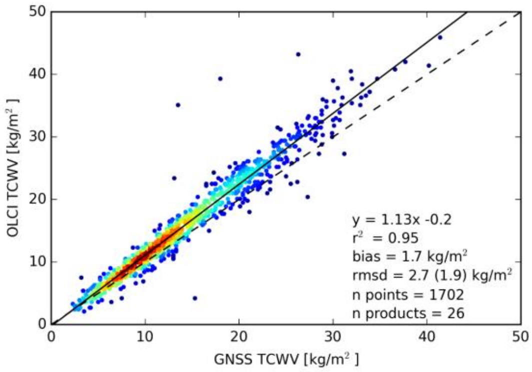

Figure 36: scatter plot of OLCI vs. in-situ IWV for the 10-11/2016 period, NRT/NTC FR data.

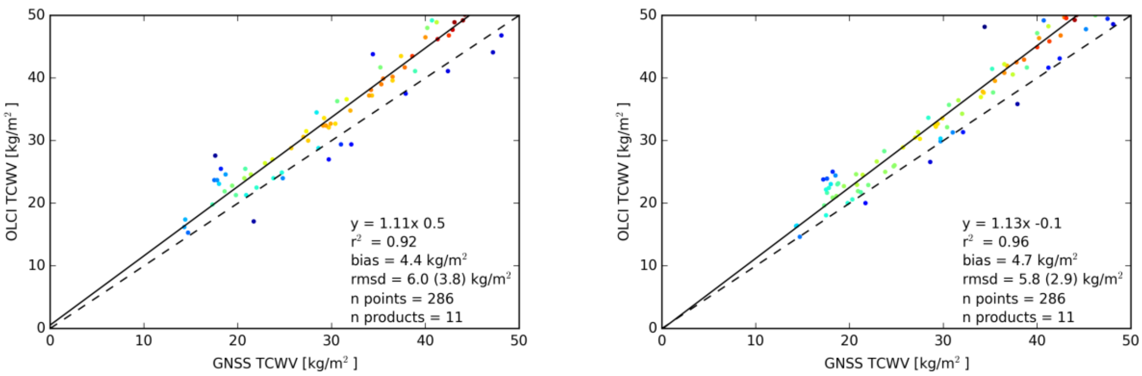

Figure 37: scatter plot of OLCI vs. in-situ IWV for the reprocessed period, FR (left) and RR (right) data.

4 Level 2 Water products validation

[OLCI-L2WLR-CV-300, OLCI-L2WLR-CV-310, OLCI-L2WLR-CV-32, OLCI-L2WLR-CV-330, OLCI-L2WLR-CV-340, OLCI-L2WLR-CV-350, OLCI-L2WLR-CV-360 and OLCI-L2WLR-CV-370] – Level 2 Water-leaving Reflectance product validation

Activities done

- The focus for this time period has been on the Near Real Time data (i.e. outdated processor).
- All extractions and statistics have been regenerated for the last two months (rolling archive limitation). A limited number of matchups are therefore available
- Only AERONET-OC in-situ data are available for this time period.

Overall Water-leaving Reflectance performance

Figure 38 on next page present the scatter plots with statistics of OLCI versus in situ reflectances computed for the NRT dataset covering the period from December 1st 2016 to March 30th 2017 dataset. A positive bias is visible particularly on 412 and 443 nm confirming the need for vicarious calibration.

Table 1 below summaries the statistics over the last NRT period, confirming the important bias at 412 and 443nm, 70% and 43% respectively, going done to about 10% toward the green bands.

Table 1: statistics over the last NRT period

lambda	N	RPD	|RPD|	MAD	RMSE	slope	int.	r2
412	25	70,55%	77,47%	0,0055	0,0071	0,9486	0,0061	0,6787
443	25	43,34%	44,27%	0,0045	0,0056	1,1251	0,0028	0,9037
490	24	28,53%	28,53%	0,0048	0,0059	1,1634	0,0016	0,9611
510	2	31,69%	31,69%	0,0091	0,0093	2,0459	-0,0207	1,0000
560	17	15,44%	16,95%	0,0037	0,0052	1,1350	0,0003	0,9655
665	25	10,56%	34,24%	0,0010	0,0032	1,3661	-0,0013	0,9236

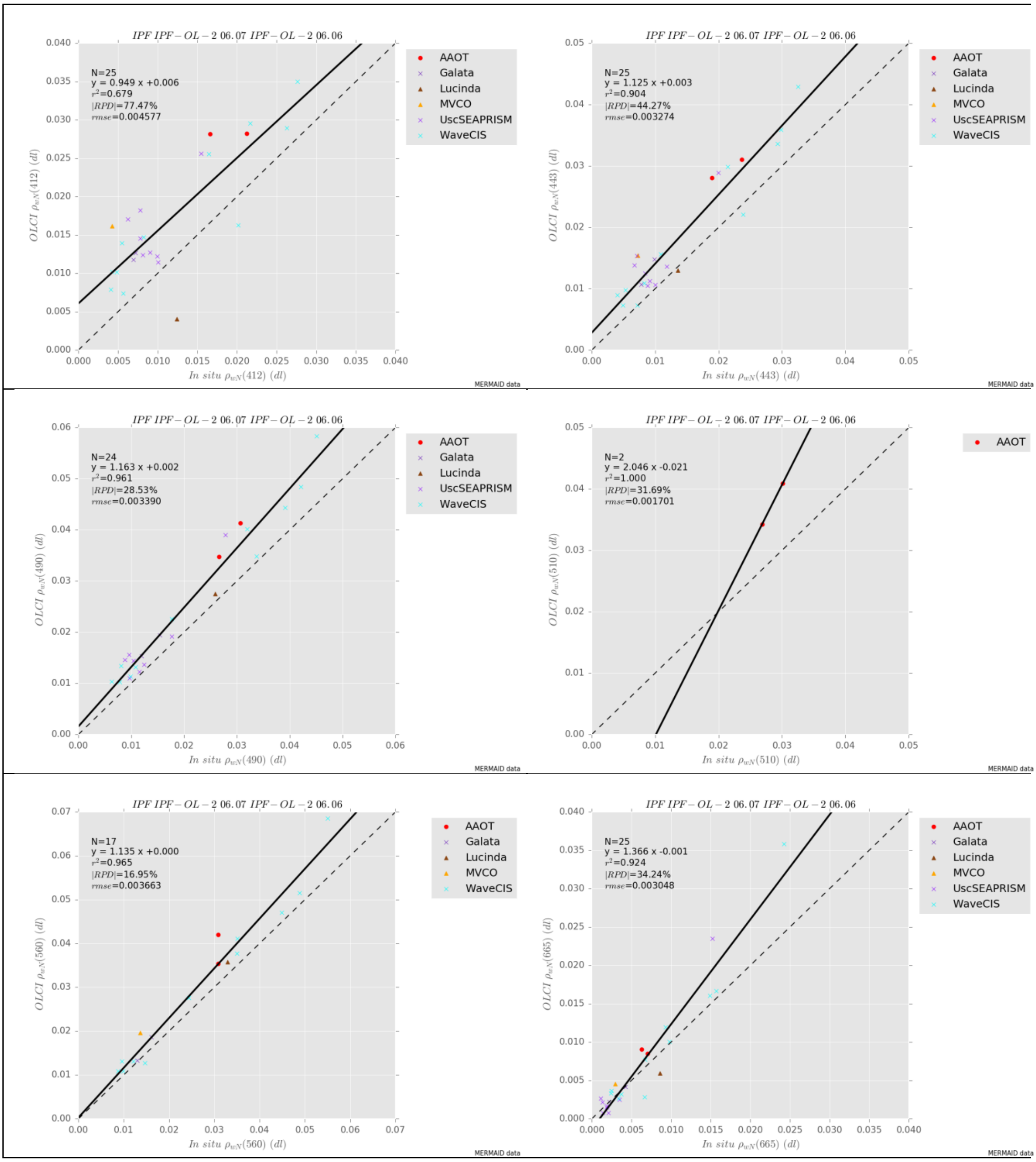

Figure 38: Scatter plots of OLCI versus in situ radiometry

Figure 39 below shows the AAOT time series derived over the December 2016 to February 2017. The general cycle on in situ data is well reproduced but OLCI products but with a clear bias (notably at 412 and 443nm).

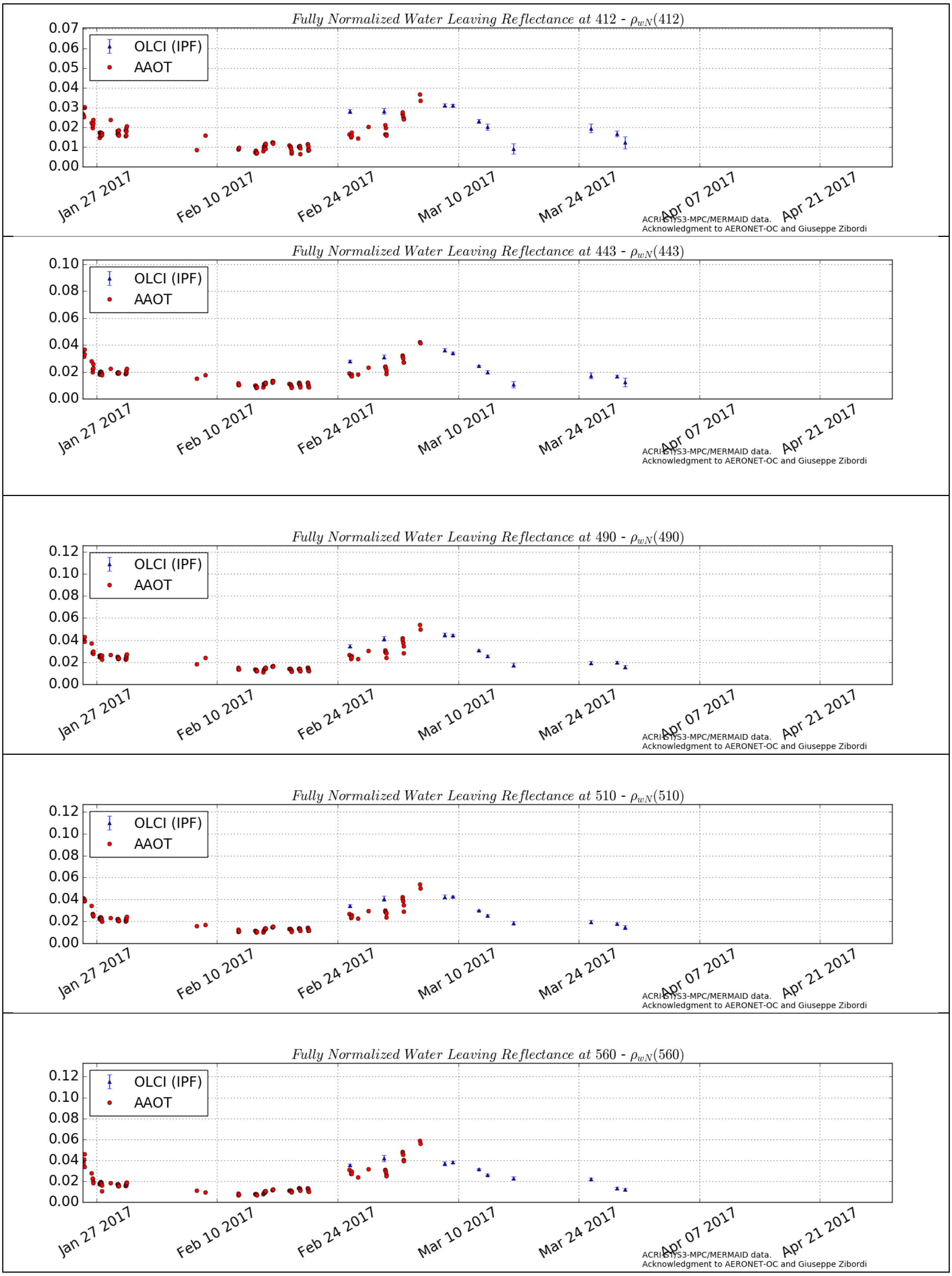

Figure 39: Radiometric time series of AAOT.

Figure 40 below shows the WaveCIS AERONET-OC station time series. The high dynamic of the last months is well captured by OLCI

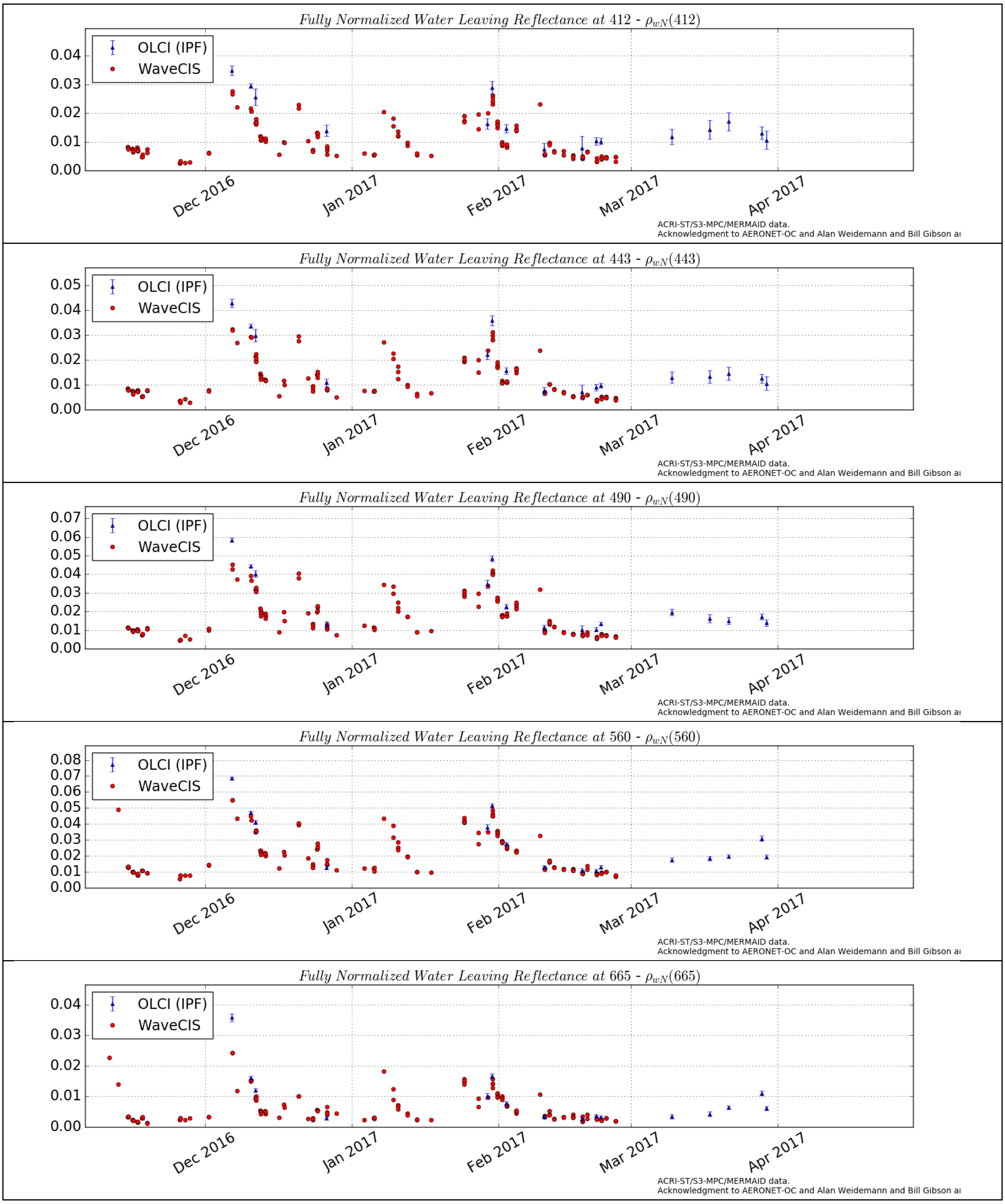

Figure 40: Radiometric time series of WaveCIS

5 Level 2 SYN products validation

[SYN-L2-CV-100]

There has been no update on SYN products validation quantitative assessment during the cycle. Last figures (cycle 10) are considered valid.

Qualitative assessment by product inspection showed no detectable performance evolution.

6 Events

Three OLCI Radiometric Calibration Sequences have been acquired during Cycle 015:

- S01 sequence on 27/02/2017 12:39 to 12:41 (absolute orbit 5372)
- S01 sequence on 12/03/2017 08:38 to 08:40 (absolute orbit 5555)
- S01 sequence on 22/03/2017 14:21 to 14:23 (absolute orbit 5701)

7 Appendix A

Other reports related to the Optical mission are:

- S3-A SLSTR Cyclic Performance Report, Cycle No. 015 (ref. S3MPC.RAL.PR.02-015)

All Cyclic Performance Reports are available on MPC pages in Sentinel Online website, at: https://sentinel.esa.int

End of document